



HAL
open science

Investigation of Spatial Scale Effects on Suffusion Susceptibility

Chuheng Zhong, van Thao Le, Fateh Bendahmane, Didier Marot, Zhen-Yu Yin

► **To cite this version:**

Chuheng Zhong, van Thao Le, Fateh Bendahmane, Didier Marot, Zhen-Yu Yin. Investigation of Spatial Scale Effects on Suffusion Susceptibility. *Journal of Geotechnical and Geoenvironmental Engineering*, 2018, 144 (9), pp.04018067. 10.1061/(ASCE)GT.1943-5606.0001935 . hal-03600144

HAL Id: hal-03600144

<https://hal.science/hal-03600144>

Submitted on 7 Mar 2022

HAL is a multi-disciplinary open access archive for the deposit and dissemination of scientific research documents, whether they are published or not. The documents may come from teaching and research institutions in France or abroad, or from public or private research centers.

L'archive ouverte pluridisciplinaire **HAL**, est destinée au dépôt et à la diffusion de documents scientifiques de niveau recherche, publiés ou non, émanant des établissements d'enseignement et de recherche français ou étrangers, des laboratoires publics ou privés.

Investigation of spatial scale effects on suffusion susceptibility

By Chuheng ZHONG¹, Van Thao LE^{2,3}, Fateh BENDAHMANE⁴,
Didier MAROT⁵, Zhen-Yu YIN⁶

¹ Chuheng Zhong, Ph.D student

Université de Nantes, Research Institute of Civil Engineering and Mechanics, CNRS
58 rue Michel Ange, BP 420
F-44606 Saint-Nazaire Cedex, France

Email : chuheng.zhong@etu.univ-nantes.fr

² Van Thao Le, Ph.D student

Université de Nantes, Research Institute of Civil Engineering and Mechanics, CNRS
58 rue Michel Ange, BP 420
F-44606 Saint-Nazaire Cedex, France

³ University of Science and Technology –The University of Danang

54 Nguyen Luong Bang Street, Lien Chieu District, Da Nang city, Vietnam

Email: van-thao.le@etu.univ-nantes.fr

⁴ Associate Professor Fateh Bendahmane

Université de Nantes, Research Institute of Civil Engineering and Mechanics, CNRS
58 rue Michel Ange, BP 420
F-44606 Saint-Nazaire Cedex, France

Email : fateh.bendahmane@univ-nantes.fr

³ Professor Didier Marot

Université de Nantes, Research Institute of Civil Engineering and Mechanics, CNRS
58 rue Michel Ange, BP 420
F-44606 Saint-Nazaire Cedex, France

Email : didier.marot@univ-nantes.fr

⁴ Associate Professor Zhen-Yu Yin

Ecole Centrale de Nantes, Research Institute of Civil Engineering and Mechanics,
CNRS

1 rue de la Noë, BP 92101,
F-44321 Nantes Cedex 3, France

Email : zhenyu.yin@ec-nantes.fr

Corresponding author: Didier Marot

Tel: 33 2 40 17 87 32 Fax : 33 2 40 17 81 60

Email: didier.marot@univ-nantes.fr

41

42 **Abstract**

43 Internal erosion processes in earth structures and their foundations may
44 increase the failure risk of such structures. Suffusion, one of the main internal
45 erosion processes, selectively erodes the fine particles which move through the
46 voids formed by the coarser particles. In literature, several suffusion susceptibility
47 investigations were already published with various tested specimen sizes.
48 However, the influence of the specimen size on suffusion susceptibility is not well
49 established. The objective of this study is to investigate this influence by comparing
50 results of suffusion tests performed on six different soils, with two different sized
51 devices. First, this study highlights the complexity of suffusion process which is a
52 combination of three processes: detachment, transport and possible filtration of the
53 finer fraction. The results also show a decrease of the critical hydraulic gradient with
54 the size of the specimen. The proposed interpretative method is based on the
55 energy expended by the seepage flow and the cumulative loss dry mass. This
56 method permits to obtain the same suffusion susceptibility classification for both
57 specimen sizes.

58

59 **Key words** : Dam safety – Suffusion – Erodimeter – Spatial scale effect – Water
60 seepage energy

61

62 INTRODUCTION

63 Soil erosion generally refers to the detachment and transport of the soil caused by
64 water flow, or wind flow. The erosion caused by a water flow can be divided into
65 internal erosion and external erosion, which are respectively related to internal
66 seepage and flow along the surface. Thus for earth structures, such as embankments,
67 dams or dikes, seepage flow can generate internal or external erosion of the soil
68 constituting the structure or its foundation which can in turn reduce significantly the
69 soil strength (Chang and Yin, 2011; Yin et al., 2014, 2016). This inherent hydro-
70 mechanical coupling, highlights the complexity of the phenomenon. Among 128 failure
71 of embankment dams, Foster et al. (2000) indicated that around 46.1% show
72 evidences of internal erosion, 48.4% are due to overtopping and 5.5% only are
73 triggered by sliding. Although erosion is one of the most common origins of failure for
74 dikes or embankment dams, it remains a recent research topic and poorly understood
75 phenomenon. Fell and Fry (2013) distinguished four forms of internal erosion: 1)
76 concentrated leak erosion, i.e. the water erodes a crack, a hole or a hollow, 2)
77 backward erosion progresses from a free surface on the downstream side of earth
78 structure towards the upstream, 3) contact erosion occurs at an interface between a
79 fine soil layer and another layer made of a coarser soil and 4) suffusion, also named
80 internal instability. This paper deals with suffusion which takes place inside the soil
81 matrix and selectively erodes the fine particles which move through the voids formed
82 by the coarser particles. Fell and Fry (2013) proposed three criteria which have to be
83 satisfied for suffusion to occur: a geometric criterion, a stress criterion and a hydraulic
84 criterion. The geometric criterion points out that the size of the fine particles must be
85 smaller than the size of the voids between the coarser particles, which compose the
86 matrix of the soil. According to the stress criterion, the fine particles should not cram

87 the space between the coarser particles and should not carry a significant amount of
88 the effective stresses. The third criterion which is related to the hydraulic loading
89 assumes that the velocity of the flow through the soil matrix must be high enough to
90 move the loose fine particles through the matrix constrictions.

91 To consider the two first criteria, the grain size distribution represents a key parameter
92 and in the past few decades, the research on soil gradation has earned much attention
93 in order to characterize the potential of suffusion. Fell and Fry (2007) concluded that
94 soils having a grain-size distribution curve either discontinuous or upwardly concave
95 are likely to suffer from suffusion. Proposals of various geometric assessment
96 methods exist in the literature, mostly based on the particle size distribution (Kenney
97 and Lau, 1985; Wan and Fell, 2008; Chang and Zhang, 2013a; among others). With
98 the purpose to take also into account the influence of the relative density, Indraratna
99 et al. (2015) proposed a criterion based on constriction size distribution.

100 The third criterion is related to the action of the fluid phase, i.e. to the seepage loading
101 required to detach and then to transport the fine particles. Skempton and Brogan
102 (1994) proposed to relate the onset of suffusion with an increase of hydraulic
103 conductivity and to characterize this hydraulic loading threshold with the hydraulic
104 gradient, termed as the critical hydraulic gradient. However, the filtration of some
105 detached particles can induce a clogging process within the soil accompanied with the
106 decrease of the hydraulic conductivity (Reddi et al. 2000; Bendahmane et al. 2008;
107 Marot et al. 2009; Nguyen et al. 2012). In consequence, Marot et al. (2016) considered
108 both the drop of hydraulic head Δh and the flow rate Q to evaluate the hydraulic
109 loading. They expressed the total power expended by the seepage flow by:

$$110 \quad P_{\text{flow}} = Q \gamma_w \Delta h \quad (1)$$

111 in which γ_w is the unit weight of water.

112 Marot et al. (2011) expressed the erosion resistance index by:

113
$$I_{\alpha} = -\log \left(\frac{m_{\text{dry}}}{E_{\text{flow}}} \right) \quad (2)$$

114 where E_{flow} is the expended energy, computed by time integration of the instantaneous
115 flow powers, and m_{dry} is the cumulative eroded dry mass. From this energy based
116 method and thanks to twenty-three tests performed with a triaxial erodimeter, six
117 categories of suffusion soil susceptibility were proposed: from highly resistant to highly
118 erodible (Marot et al., 2016).

119 For characterizing the initiation and the development of suffusion, most experimental
120 devices comprise a rigid wall cylinder (Kenney and Lau, 1985; Skempton and Brogan,
121 1994; Wan and Fell, 2008; Sail et al. 2011). To investigate suffusion under complex
122 stress states and to minimize probable side wall leakage, Bendahmane et al. (2008),
123 and more recently, Chang and Zhang (2011) developed a specific triaxial cell,
124 designed to force the fluid to percolate throughout the sample. This variation in testing
125 devices is accompanied by various tested specimen sizes: diameters from 50 mm to
126 300 mm and heights from 50 mm to 600 mm. However, the potential influence of the
127 specimen volume on suffusion susceptibility has not been well established. Thus, this
128 paper aims to investigate this spatial scale influence by comparing results of suffusion
129 tests performed with two different-sized devices. A campaign of suffusion tests is
130 performed on gap graded and widely graded soils. For each tested soil, the results are
131 discussed in terms of suffusion susceptibility (Marot et al., 2016). Specimens of
132 different sizes are compared provided that their initial hydraulic conductivity are
133 similar.

134 **LABORATORY EXPERIMENTS**

135 **Main characteristics of testing devices**

136 Two different apparatuses were designed to perform suffusion tests with a flow in a
137 downward direction. The larger device, named as oedopermeameter is composed of
138 a 285 mm inner diameter rigid wall cylinder cell, and the specimen height can reach
139 600 mm (see Figure 1(a)). The second device consists essentially of a modified triaxial
140 cell. Specimen sizes are 50 mm in diameter and up to a 100 mm in height (see Figure
141 1(b)). A detailed description of each device was reported by Sail et al. (2011) and by
142 Bendahmane et al. (2008) respectively, however, a brief summary is provided here.
143 For both devices, the fluid circulates into the top cap which contains a layer of gravel
144 or glass beads to diffuse the fluid flow uniformly on the specimen top surface. Both
145 cell bases have a vertical funnel-shaped draining system, specially designed to avoid
146 clogging. Each draining system is connected to a collecting system which is composed
147 of an effluent tank containing a rotating support with eight beakers to catch the eroded
148 particles during testing. With the objective to test specimens in oedometric condition
149 with both devices, the membrane of the triaxial erodimeter is surrounded by a steel
150 mold. However, due to the different weights of specimens and top caps in both
151 devices, the vertical effective stress at the specimen bottom is 5.9 kPa greater in the
152 oedopermeameter. In both devices, the specimen is placed on a sieve with 1.2 mm
153 pore opening size which is fixed on a 10 mm mesh screen. According to the apparatus
154 used, the range of flow rate varies, thus two configurations are used: a flowmeter is
155 used in the case of the oedopermeameter, whereas at the overflow outlet of the triaxial
156 erodimeter, water falls in a beaker which is continuously weighed. The hydraulic
157 controlled system is composed of a pressure controller connected to two 200 L tanks,

158 alternatively used in the oedopermeameter apparatus and one upstream water tank
159 for the triaxial erodimeter. The differential pore water pressure across the specimen is
160 measured using a differential pressure transducer connected to the top cap and the
161 pedestal base for the triaxial erodimeter. The rigid wall of the oedopermeameter cell
162 is equipped with twelve pressure ports; in addition a pressure port is placed on the
163 piston base plate (i.e. at the specimen-piston interface) and a fourteenth one is located
164 below the specimen on top of the funnel-shaped drainage system. All these pressure
165 ports are connected to a multiplex unit itself connected to a manometer to avoid
166 discrepancy. For each device, a dedicated computer operates the data acquisition
167 thanks to a LabVIEW program developed by the authors.

168 **Testing materials**

169 A laser diffraction particle-size analyser was used to measure the grain size
170 distribution of the tested soils (see Figure 2). Tests were performed with demineralised
171 water and without using a deflocculation agent. Two types of gradations were selected,
172 gap graded and widely graded. The four gap-graded soils were composed of either
173 sand and gravel (numbered 1, 4 and 6) or silt, sand and gravel (number 5). The
174 gradations of these four gap-graded soils differed slightly, mainly with respect of the
175 fines content ranging from 16.5% to 25%. Considering the two widely graded soils, the
176 cohesionless one is composed of silt, sand and gravel (number 3) and the clayey one
177 (number 2) is composed of 25% of Kaolinite Proclay and 75% of Fontainebleau sand.
178 All these soils were selected in order to obtain internally unstable soils. According to
179 grain size based criteria proposed by Kenney and Lau (1985) and Indraratna et al.
180 (2015), all these soils are, indeed internally unstable (see Table 1). However, since
181 the percentage of fines P is higher than 20% for soil 2 and the gap ratio G_r is smaller

182 than 3 for soil 4, these two soils are classified as internally stable by Chang and
183 Zhang's (2013a) method. Wan and Fell's (2008) method seems not applicable for gap-
184 graded soils nor for soils with a mass of fine fraction lower than 15 %. Hence, this
185 method is only relevant for soil 3 which is classified as internally stable.

186 **Specimen preparation and testing program**

187 For clarity, the first number of each test name is related to the gradation (Fig. 2). The
188 letter indicates the apparatus used: O for the oedopermeameter test and T for the
189 triaxial erodimeter test, and the last number indicates the specimen number.

190 For each soil, the whole quantity for both tests was prepared at the same time to avoid
191 segregation and discrepancy. The first step of specimen preparation consists in
192 moistening the soil with a water content of about 8% and mixing thoroughly. Within the
193 oedopermeameter cell, the specimens were placed in three layers and each layer was
194 compacted to reach a fixed initial dry density. For triaxial erodimeter tests, the
195 specimens were prepared using a single-layer semi-static compaction technique,
196 again targeting a prescribed initial dry density. For both devices, carbon dioxide was
197 upwardly injected to improve dissolution of gases into water, and finally, upward
198 saturation was completed by adding demineralized water. This step was performed
199 with a low hydraulic gradient by increasing the level of the dedicated water tank (see
200 Fig. 1(a) and 1(b)), until the water reached the air release valve. Two saturation
201 procedures were tested for both devices to saturate specimens using the same
202 duration or with the same wetting front velocity.

203 A beaker was systematically used to catch the loss of particles during the saturation
204 phase. The dry mass was measured after drying the collected particles at 105°C for

205 24 hours. The order of magnitude of dry mass loss increases with the specimen
206 volume and the accuracy of dry mass measurement is evaluated to ± 2 mg for the
207 triaxial erodimeter test and ± 0.02 g for the oedopermeameter test.

208 Table 2 summarises the initial lengths and the initial dry densities of each sixteen
209 tested specimens.

210 For soil 6, two specimens were prepared for each device using the same initial dry
211 density (see Table 2). The percentage of particles lost during the saturation step is
212 expressed as the ratio of lost particle mass over the initial mass of fines in the
213 specimen. Figure 3 shows the great influence of this percentage on the initial hydraulic
214 conductivity. Moreover, it was observed that the loss of particles increased with the
215 wetting front velocity. In consequence, the saturation of specimens was systematically
216 applied for both devices under the same wetting front velocity to limit the discrepancy
217 in the initial hydraulic conductivity which is also indicated in Table 2.

218 Rochim et al. (2017) showed that the history of hydraulic loading has a significant
219 influence on the development of suffusion, and with the objective of following the
220 development of all possible combinations, tests must be carried out by increasing the
221 applied hydraulic gradient. Thus in this study, specimens were systematically tested
222 under a multi-staged hydraulic gradient (see Table 2) and each stage lasted thirty
223 minutes. The total duration of each test is detailed in Table 2. A beaker was used to
224 catch the eroded particles during each hydraulic gradient stage and the corresponding
225 dry masses were measured.

226 Moreover, after each oedopermeameter test, the quantity of detached particles was
227 large enough to perform one accurate grain size distribution; in addition, each eroded

228 specimen was divided into four layers (see Fig. 1(a)) to determine the post suffusion
229 test gradations. Finally, the repeatability of our specimen preparation and testing
230 procedure was verified by performing 2 tests under identical conditions: 6-O-1 and 6-
231 O-2.

232 **RESULTS**

233 **Post-test particle size distributions of specimens**

234 Figures 4(a) and 4(b) show the initial gradation and gradation of the post suffusion
235 specimen, divided into four layers, for specimens 1-O and 4-O respectively. For both
236 specimens, it can be noted that the loss of fine particles is slightly larger in the
237 upstream part of the specimen in comparison with middle part. This result is in
238 agreement with results of Ke and Takahashi (2012). The transport of detached
239 particles from upstream to downstream parts can partly offset the loss of particles in
240 the downstream part. For layer 4 (i.e. at the specimen's downstream part), the final
241 percentage of fines exceeds the initial percentage for specimen 1-O, whereas it is
242 lower than the initial percentage for specimen 4-O. It is worth stressing that the final
243 percentage of fine particles in layer 1 (i.e. at the specimen's upstream part) represents
244 only 64% of the initial fine percentage of fines in specimen 1-O, but about 87% in the
245 specimen 4-O. In consequence, the filtration which appears obvious in specimen 1-O
246 seems to be raised by the amount of detached particles.

247 **Grain size distribution of eroded particles**

248 Only a few data exist in the literature concerning the grain size distribution of eroded
249 particles during the process of suffusion. Thanks to the collecting system of the
250 oedopermeameter, the eroded soils are caught separately at different stages. Fig. 5

251 displays the grain size distribution of eroded particles for test 1-O at each loading
252 stage. The sieve under the specimen has a 1.2 mm pore opening size and therefore
253 allows the migration of all particles of the finer fraction. As the maximum diameter of
254 the finer fraction of this soil is 0.8 mm (see Figure 2), Fig. 5 shows that even coarser
255 particles of finer fraction can be eroded. From the first stage of the hydraulic gradient
256 ($i = 0.042$) to the fourth one ($i = 0.250$), the maximum grain size increases. This
257 evolution seems to show that the suffusion process first concerns only the finest
258 particles of the finer fraction and progressively, all sizes of the finer fraction. However,
259 during the last two stages, the maximum grain size of detached particles decreases.
260 In consequence, the time evolution of the grain size distribution of detached particles
261 combined with the spatial variation of the specimen's grain size distribution highlights
262 the complexity of suffusion process which appears as a combination of three
263 processes: detachment, transport and possible filtration of the finer fraction.

264 **Rate of erosion and hydraulic conductivity**

265 Reddi et al. (2000) expressed the erosion rate of soils per unit pore area (\dot{m}) by:

$$266 \quad \dot{m} = \frac{m(\Delta t)}{N_p S_p \Delta t} \quad (3)$$

267 where m is the eroded dry mass during the elapsed time Δt , N_p is the number of
268 equivalent pores and S_p the equivalent pore area. Reddi et al. (2000) assumed that
269 the equivalent radius r is representing the effects of all pores and is defined by:

$$270 \quad r = \sqrt{\frac{8 k \eta}{n \gamma_w}} \quad (4)$$

271 where k is the hydraulic conductivity, η the dynamic viscosity and n the porosity.

272 N_p and S_p can be computed respectively by:

273
$$N_p = \frac{S n}{\pi r^2} \quad (5)$$

274
$$S_p = 2 \pi r L \quad (6)$$

275 where S is the cross section area of the specimen and L is the length of the specimen.

276 Hence, the erosion rate per unit pore area depends both on the hydraulic conductivity

277 and the porosity, which evolve in time. During the suffusion process, the

278 measurements show that the maximum value of axial strain did not exceed 0.56%

279 (maximum axial strain of 0.558% was obtained for test 3-O). In consequence, for the

280 computation of porosity during the testing time, the specimen height is assumed

281 constant and sole the eroded dry mass measurement is taken into account.

282 For tests on soil 3, Figures 6(a) and 6(b) show the time evolution of the hydraulic

283 conductivity and the time evolution of the erosion rate per unit pore area, respectively.

284 The results in these figures are rather scattered. It is worth noting that the imprecision

285 regarding the hydraulic conductivity computation is estimated at $\pm 3.5 \cdot 10^{-6} \text{ m.s}^{-1}$ and

286 $\pm 0.8 \cdot 10^{-6} \text{ m.s}^{-1}$, for the triaxial erodimeter and the oedopermeameter respectively.

287 Similarly, the accuracy of the erosion rate measurement is estimated at $\pm 3 \cdot 10^{-11} \text{ kg.s}^{-1}$.

288 m^{-2} . Thus those spread out results cannot be attributed to imprecision but rather to

289 the complexity of the suffusion process. In the case of soil 3, as for soils 1, 4, 5 and 6,

290 the hydraulic conductivity and the rate of erosion stay relatively constant during

291 suffusion tests with both devices.

292 For soil 2, the hydraulic conductivity first decreases (see Fig. 7(a)). However, for test

293 2-T when the applied hydraulic gradient was increased from 3.8 to 5.8, the hydraulic

294 conductivity sharply increased. This sudden increase is accompanied by an increase

295 of the erosion rate (see Fig. 7(b)) and sand grains are detected in the effluent. In

296 consequence, this erosion process can be named global backward erosion. During
297 tests 2-O-1 and 2-O-2, a sudden increase in hydraulic conductivity could be also
298 measured when the applied hydraulic gradient reached 11 and 13 respectively, yet
299 this increase was immediately followed by a decrease. At the same time, the erosion
300 rate stayed relatively constant and a settlement was detected (the final axial strain
301 reached 1.48% for test 2-O-1 and 8.52% for test 2-O-2). It is worth noting that the
302 effective stress applied on oedopermeameter specimens was larger than that on
303 triaxial erodimeter specimens due to the weight of each piston and the specimen's
304 weight. In tests performed with the oedopermeameter, the effective stress at the
305 bottom of the specimen can reach 8.4 kPa, whereas, in test 2-T, the effective stress
306 is about 2.5 kPa. Thus for the soil 2, a slight rise of the effective stress seems to avoid
307 the onset of global backward erosion and only clay suffusion is detected. This
308 emphasis on the influence of the effective stress on suffusion development is in good
309 agreement with the results obtained by Moffat and Fannin (2006) who showed that a
310 rise in the effective stress causes an increase in the soils' resistance to suffusion.
311 For each test, the simultaneous stabilization of the hydraulic conductivity and the rate
312 of erosion is highlighted by a black spot (see Fig. 6(a), 6(b), 7(a) and 7(b)). The
313 corresponding time is interpreted as at the end of the suffusion.

314 **Discussion**

315 **Onset of suffusion**

316 In literature, several studies restricted suffusion characterization to the initiation of the
317 process. Three methodologies are used in order to detect the suffusion onset: (i) the
318 increase of erosion rate (Chang and Zhang, 2013b), (ii) the variations of local hydraulic
319 gradient (Moffat and Fannin, 2006) or (iii) the increase of hydraulic conductivity

320 (Skempton and Brogan, 1994). To date, those methodologies suffer from various
321 limitations.

322 (i) Rochim et al. (2017) highlighted that according to the type of hydraulic
323 loading (i.e. tests performed under hydraulic gradient controlled conditions
324 or under flow rate controlled conditions), the predominant process can be
325 either filtration or erosion. Moreover under a multi-staged hydraulic gradient,
326 these results show that the rate of erosion is influenced by the increment of
327 the applied hydraulic gradient and the duration of each stage. Based on
328 these results, it seems to be difficult to define the onset of suffusion by a
329 threshold of erosion rate independently of the hydraulic loading history.

330 (ii) Moffat and Fannin (2006) assumed that the onset of large erosion of fine
331 particles is governed by a significant drop of a hydraulic gradient that they
332 named local hydraulic gradient. It is worth noting that the vertical spacing
333 between ports for the measurement of this hydraulic gradient was 125 mm,
334 which represents 625 times the diameter of the coarser grains of tested finer
335 fraction. Sail et al. (2011) showed that a significant drop of local hydraulic
336 gradient can be preceded by a variation of local hydraulic head in another
337 part of the specimen. These results indicate that the onset of suffusion does
338 not concern the whole specimen but is a localized process, and that its
339 detection strongly depends on the position of the pressure sensors.

340 (iii) The third method of detecting the onset of suffusion is based on the variation
341 of the hydraulic conductivity. The advantage of this method is related to
342 spatial scale of the characterization as it is realized at specimen scale. The
343 flow velocity versus the hydraulic gradient is plotted in Figure 8(a) for tests
344 on soil 1 and in Figure 8(b) for tests on soil 3. With the objective to determine

345 with accuracy the onset of suffusion, the relative evolution of the hydraulic
346 conductivity is computed and the onset of suffusion is systematically defined
347 by the first relative increase of 10%. The corresponding value of the
348 hydraulic gradient is determined by linear interpolation and selected as the
349 critical hydraulic gradient (see Fig. 8(a)). As shown by test 3-O in Fig. 8(b),
350 the determination of the critical hydraulic gradient with this systematic
351 approach is not possible for all realized tests. When this approach can be
352 used, the values of the critical hydraulic gradient are indicated in Table 3.
353 According to the authors, the pitfall of this method lies in the description of
354 the hydraulic loading based on the hydraulic gradient. In fact, Figure 9
355 shows that the critical hydraulic gradient decreases with the specimen
356 length, with a ratio between 1.15 (soil 1) and 1.73 (soil 4). It is worth noting
357 that the specimen length corresponds to the seepage path in the case of a
358 vertical seepage flow. This decrease of the critical hydraulic gradient with
359 seepage length is in agreement with expressions of critical hydraulic
360 gradient proposed by Li (2008) for suffusion process and by Sellmeijer
361 (1988) for backward erosion piping process. Moreover, thanks to a
362 centrifuge bench Marot et al. (2012) showed that even under a controlled
363 effective stress, the critical hydraulic gradient decreases with the length of
364 the seepage path.

365 The interpretative method based on the critical hydraulic gradient assumes that the
366 hydraulic gradient is independent of the considered spatial scale, and the soil is
367 expected to remain homogenous all along the considered flow path. On the contrary,
368 post suffusion gradations (see Figures 4(a) and 4(b)) show that the soil rapidly
369 becomes heterogeneous, i.e. some grains are detached, others are blocked and a few

370 are transported. In addition, it is worth noting that the spatial distribution of these
371 mobilized grains is not homogenous all along the seepage path so that the head losses
372 also are heterogeneous. Now if we consider the interstitial overpressure at the scale
373 of several grains, which induces the suffusion onset, it represents the main component
374 of the head losses along the considered flow path. The spacing between ports for
375 hydraulic gradient measurement represents several hundred times the diameter of the
376 finer grains. So this hydraulic gradient decreases with the considered length of the
377 flow path. In other words, for a given local overpressure, the hydraulic gradient
378 decreases with the length of flow path. Consequently, the value of critical hydraulic
379 gradient determined by laboratory tests can be larger by several orders of magnitude
380 than any value predicted for the real scale. It is worth stressing that this interpretative
381 method based on the critical hydraulic gradient, which decreases with seepage path
382 length, is completely opposite with the risk assessment.

383 **Erosion coefficient**

384 Based on the Reddi et al. (2000) concept of a system of parallel capillary tubes to
385 represent a porous medium, Marot et al. (2016) expressed the hydraulic shear stress
386 by:

$$387 \quad \tau = \left(\frac{\Delta h}{\Delta z} \right) \sqrt{\frac{2 k \eta \gamma_w}{n}} \quad (7)$$

388 where Δh is the drop of the hydraulic head between an upstream section A and a
389 downstream section B, $\Delta z = z_A - z_B$, z_A and z_B are altitudes of sections A and B
390 respectively.

391 Figures 10(a) and 10(b) show the erosion rate per unit pore area (Eq. 3) versus the
392 hydraulic shear stress (Eq. 7) for soils 1 and 3 respectively. The suffusion development
393 phase starts from the suffusion onset which is defined thanks to the aforementioned

394 identification based on hydraulic conductivity increase. The commonly used
395 interpretative method for hole erosion tests (Wan and Fell, 2004) consists in describing
396 the erosion rate from the linear excess shear stress equation, and the slope of this
397 equation corresponds to the erosion coefficient. As shown by test 3-T in Fig 10(b), it
398 is not possible to determine the erosion coefficient for all suffusion tests. Table 3
399 details the obtained values of erosion coefficient. It is worth noting that the values
400 determined thanks to the oedopermeameter tests are systematically larger than
401 results obtained with the triaxial erodimeter. Thus the characterization of suffusion
402 susceptibility based on this interpretative method depends on specimen size.

403 **Energy based method**

404 As already mentioned, the authors consider that the suffusion induces several
405 heterogeneities by the combination of detachment, transport and possible filtration of
406 the finer fraction. From this perspective, the authors propose to use the power
407 expended by the seepage flow P_{flow} computed by Eq. 1, for characterizing the hydraulic
408 load which produces these combined effects at the specimen spatial scale. Moreover,
409 with the objective of taking the history of hydraulic loading into account, the energy
410 expended by the seepage flow E_{flow} is determined by the time integration of total flow
411 power for the test duration. Rochim et al. (2017) showed that at the end of the suffusion
412 process, i.e. the stabilization of both the hydraulic conductivity and the erosion rate
413 (see Figures 6(a), 6(b), 7(a) and 7(b)), the value of the erosion resistance index (Eq.
414 2) can be determined with accuracy for different hydraulic loadings. In consequence,
415 for characterizing the erosion susceptibility, the erosion resistance index is computed
416 at this stabilization time.

417 Figure 11 shows the cumulative expended loss dry mass versus the cumulative
418 expended energy for all tests performed with both devices. First, this figure shows that
419 repeatability is fairly good, as the two representation points of tests 6-O-1 and 6-O-2
420 are very close. Moreover, it is worth noting that the value of the erosion resistance
421 index can be determined with accuracy for the different specimen sizes (see Table 4).
422 The expended energy depends on the specimen size but also the eroded dry mass.
423 Therefore, the erosion resistance index (i.e. which corresponds to the ratio of these
424 two parameters) does not depend on the specimen size and the suffusion
425 susceptibility classification is the same for both devices. I_{α} is between 2.89 and 2.94
426 for tests on soil 1 (i.e. this soil is Erodible according to the suffusion susceptibility
427 classification proposed by Marot et al., 2016), between 4.22 and 4.48 for soil 2
428 (Moderately Resistant), between 4.64 and 4.73 for soil 3 (Moderately Resistant),
429 between 3.06 and 3.26 for soil 4 (Moderately Erodible), between 3.36 and 3.92 for soil
430 5 (Moderately Erodible) and between 2.95 and 3.70 for soil 6 (Erodible, Moderately
431 Erodible).

432 Finally, it can be observed that for soils 1, 5 and 6, all the grain size distribution criteria
433 used give an indication of internal instability and the suffusion susceptibility
434 classification is Erodible or Moderately Erodible. Whereas for soils 2, 3 and 4, the
435 conclusions of the grain size distribution based criteria are opposite and the suffusion
436 susceptibility classification permits distinction of the tested soils, from Moderately
437 Erodible (soil 4) to Moderately Resistant (soils 2 and 3).

438 **Conclusion**

439 In this study, a series of suffusion tests were carried out with two different-sized
440 devices to assess the suffusion susceptibility of six gradations. Sixteen specimens

441 including widely-graded, gap-graded, clayey and cohesionless soils were tested
442 involving seepage flow in a downward direction under multi-stage hydraulic gradient
443 condition.

444 First a loss of particles was observed during the saturation phase even under upward
445 flow. Thus to limit the discrepancy in the initial hydraulic conductivity, a systematic
446 saturation approach, adopting the same velocity of the wetting front was applied to
447 both devices.

448 The post-suffusion gradations and size distribution of eroded particles highlight the
449 complexity of suffusion which appears as the combination of detachment-filtration-
450 transport processes. Due to this coupling between erosion and filtration, the time
451 evolutions of the hydraulic conductivity and of the erosion rate can be complex.

452 The method to identify the critical hydraulic gradient based on the increase of hydraulic
453 conductivity cannot be used for all specimens. Moreover the values of the critical
454 hydraulic gradient decrease with the length of the seepage path. The interpretative
455 method can also consist in describing the erosion rate by using the excess shear
456 stress equation. However, in the case of suffusion, the erosion coefficient increases
457 with specimen size.

458 An energy-based method is applied to study the suffusion susceptibility of tested
459 specimens. The energy expended by the water seepage and the cumulative loss dry
460 mass are computed until the simultaneous invariability of the hydraulic conductivity
461 and the erosion rate are reached. At this time, the erosion susceptibility classification
462 can be evaluated by the value of the erosion resistance index which lies in the same
463 range for both used devices.

464 Finally, for the clayey soil tested, under low effective stress, suffusion development
465 can induce backward erosion. Further studies are required to confirm this result for
466 other soils.

467

468 **ACKNOWLEDGEMENT**

469 The authors thank the China Scholarship Council, the company IMSRN France, the
470 Ministry of Education and Training of Vietnam and the University of Danang Vietnam
471 for providing financial support for this work.

472 **REFERENCES**

- 473 Bendahmane, F., Marot, D. and Alexis, A. (2008). "Experimental parametric Study of
474 Suffusion and Backward Erosion." *J. Geotech. Geoenviron. Eng.*, 134(1), 57-67.
- 475 Chang, D.S. and Zhang, L.M. (2011). "A Stress-controlled erosion apparatus for
476 studying internal erosion in soils." *J. ASTM Geotech Test.*, 34(6), 579-589
- 477 Chang, C.S. and Yin, Z.-Y. (2011). "Micromechanical modeling for behavior of silty
478 sand with influence of fine content." *Int J Solids Struct*, 48(19), 2655-2667.
- 479 Chang, D.S. and Zhang, L.M. (2013a). "Extended internal stability criteria for soils
480 under seepage." *Soils Found.*, 53(4), 569-583.
- 481 Chang D.S., and Zhang, L.M. (2013b). "Critical hydraulic gradients of internal erosion
482 under complex stress states." *Journal of Geotechnical and Geoenvironmental*
483 *Engineering*, 139(9), 1454-1467.
- 484 Fell, R., and Fry, J. J. (2007). *Internal erosion of dams and their foundations*, Taylor &
485 Francis, London.
- 486 Fell, R., and Fry, J. J. (2013). *Erosion in geomechanics applied to dams and levees*,
487 S. Bonelli Ed., ISTE—Wiley, London, 1–99.

- 488 Foster, M., Fell, R., and Spannagle, M. (2000). "The statistics of embankment dam
489 failures and accidents." *Can. Geotech. J.*, 37, 1000–1024.
- 490 Indraratna, B., Israr J. and Rujikiatkamjorn, C. (2015). "Geometrical method for
491 evaluating the internal instability of granular filters based on constriction size
492 distribution." *J. Geotech. Geoenviron. Eng.*, 141(10), 04015045.
- 493 Ke, L. and Takahashi, A. (2012). "Strength reduction of cohesionless soil due to
494 internal erosion induced by one dimensional upward seepage flow." *Soils Found.*,
495 52(2012), 698–711.
- 496 Kenney, T.C. and Lau, D. (1985). "Internal stability of granular filters". *Can. Geotech.*
497 *J.*, 22, 215-225.
- 498 Li, M. (2008). "Seepage induced instability in widely graded soils." PhD thesis,
499 University of British Columbia, Vancouver, Canada.
- 500 Marot, D., Bendahmane, F., Rosquoët, F. and Alexis, A. (2009). "Internal flow effects
501 on isotropic confined sand-clay mixtures." *Soil & Sediment Contamination, an*
502 *International Journal*, 18(3), 294-306.
- 503 Marot, D., Regazzoni, P.L. and Wahl, T. (2011). "Energy based method for providing
504 soil surface erodibility rankings." *J. Geotech. Geoenviron. Eng.*, 137(12), 1290-
505 1294.
- 506 Marot, D., Le, V.D., Garnier, J., Thorel, L. and Audrain, P. (2012). "Study of scale effect
507 in an internal erosion mechanism." *European Journal of Environmental and Civil*
508 *Engineering*, 16(1), 1–19.
- 509 Marot, D., Rochim, A., Nguyen, H.H., Bendahmane, F. and Sibille L. (2016).
510 "Assessing the susceptibility of gap graded soils to internal erosion: proposition of
511 a new experimental methodology." *Nat. Hazards*, 83(1), 365-388.

- 512 Moffat, R. and Fannin, J. (2006). "A large permeameter for study of internal stability in
513 cohesionless soils." *J. ASTM Geotech Test.*, 29(4), 273-279.
- 514 Nguyen, H.H., Marot, D. and Bendahmane, F. (2012). "Erodibility characterisation for
515 suffusion process in cohesive soil by two types of hydraulic loading." *La Houille*
516 *Blanche, International Water Journal*, 6, 54-60.
- 517 Reddi, L.N., Lee, I. and Bonala, M.V.S. (2000). "Comparison of internal and surface
518 erosion using flow pump test on a sand-kaolinite mixture." *J. ASTM Geotech Test.*,
519 23(1), 116-122.
- 520 Rochim, A., Marot, D., Sibille, L. and Le, V.T. (2017). "Effect of hydraulic loading
521 history on the characterization of suffusion susceptibility of cohesionless soils." *J.*
522 *Geotech. Geoenviron. Eng.*, 10.1061/(ASCE)GT.1943-5606.0001673.
- 523 Sail, Y., Marot, D., Sibille, L., and Alexis, A. (2011). "Suffusion tests on cohesionless
524 granular matter." *European Journal of Environmental and Civil Engineering*, 15(5),
525 799-817.
- 526 Sellmeijer, J.B. (1988). "On the mechanism of piping under impervious structures."
527 PhD thesis, Delft University of Technology, Netherlands.
- 528 Skempton, A.W. and Brogan, J.M. (1994). "Experiments on piping in sandy gravels."
529 *Géotechnique*, 44(3), 440-460.
- 530 Wan, C.F. and Fell, R. (2004). "Investigation of rate of erosion of soils in embankment
531 dams." *J. Geotech. Geoenviron. Eng.*, 130(4), 373-380.
- 532 Wan, C.F. and Fell, R. (2008). "Assessing the potential of internal instability and
533 suffusion in embankment dams and their foundations." *J. Geotech. Geoenviron.*
534 *Eng* 134(3), 401-407.
- 535 Yin, Z.-Y., Zhao, J. and Hicher, P.Y. (2014). "A micromechanics-based model for sand-
536 silt mixtures." *Int J Solids Struct*, 51(6), 1350–1363.

537 Yin, Z.-Y., Huang, H.W. and Hicher, P.Y. (2016). "Elastoplastic modeling of sand-silt
538 mixtures." *Soils Found.*, 56(3), 520-532.

539

540 **FIGURE CAPTIONS**

541 **Fig. 1** Sketch of the experimental benches (a) oedopermeameter; (b) triaxial
542 erodimeter

543 **Fig. 2** Grain size distribution of tested soils

544 **Fig. 3** Initial hydraulic conductivity versus percentage of loss particles for tests on soil
545 6

546 **Fig. 4** Initial soil gradation and post suffusion gradations of (a) specimen 1-O; (b)
547 specimen 4-O

548 **Fig. 5** Grain size distribution of eroded particles for test 1-O

549 **Fig. 6** Time evolution of (a) the hydraulic conductivity; (b) the erosion rate per unit pore
550 area soil 3

551 **Fig. 7** Time evolution of (a) the hydraulic conductivity; (b) the erosion rate per unit pore
552 area soil 2

553 **Fig. 8** Flow velocity versus hydraulic gradient, critical hydraulic gradients for (a) soil 1;
554 (b) soil 3

555 **Fig. 9** Critical hydraulic gradient versus specimen length

556 **Fig. 10** Erosion rate per unit pore area versus hydraulic shear stress for (a) soil 1; (b)
557 soil 3

558 **Fig. 11** Cumulative loss dry mass versus cumulative expended energy, suffusion
559 susceptibility classification. HR = Highly Resistant; R = Resistant;
560 MR = Moderately Resistant; ME = Moderately Erodible; E = Erodible;
561 HR = Highly Erodible

562

563

564 **Table 1** Properties of Tested Gradations

Properties	Tested gradations					
	1	2	3	4	5	6
P (%)	0.91	25.94	12.02	0.21	3.34	0.99
G _r	3.33	3.61	WG	2.29	9.43	3.33
C _u	15.70	67.68	22.16	7.06	43.70	16.24
d ₁₅ /d ₈₅	0.083	0.018	0.031	0.169	0.022	0.076
(H/F) _{min}	0.161	0.110	0.446	0.600	0	0.155
D (H/F) _{min} (mm)	0.494	0.030	0.606	0.490	0.414	0.494
$D_{c35}^c/d_{85,SA}^f$	2.773	14.251	17.411	1.273	6.503	2.773
Kenney and Lau's criterion	U	/	U	U	U	U
Wan and Fell's criterion	/	/	S	/	/	/
Chang and Zhang's criterion	U	S	U	S	U	U
Indraratna's criterion	U	U	U	U	U	U

565

566 Note: P = percentage of particle smaller than 0.063mm; G_r = d_{max}/d_{min} (d_{max} and d_{min}:
567 maximal and minimal particle sizes characterizing the gap in the grading curve);
568 C_u = uniformity coefficient; d₁₅ and d₈₅ are the sieve sizes for which 15% and 85%
569 respectively of the weighed soil is finer; F and H are the mass percentages of the

570 grains with a size, lower than a given particle diameter d and between d and $4d$
571 respectively; $D (H/F)_{\min}$ is the corresponding diameter with the minimum value of ratio
572 H/F ; D_{c3}^c is the controlling constriction for coarser fraction from constriction size
573 distribution by surface area technique; $d_{85,SA}^f$ is the representative size for finer fraction
574 by surface area technique; WG = widely graded soil; U = unstable; S = stable;
575 / = method not relevant for considered soil.
576

577 **Table 2** Properties of Tested Specimens and Summary of Testing Program

Specimen reference in paper	Specimen length (mm)	Initial dry density γ_d (kN/m ³)	Applied hydraulic gradient i	Initial hydraulic conductivity 10^{-3} (m/s)	Test duration (min)
1-O	425	16.50	From 0.04 to 0.23	2.02	134
1-T	100	16.43	From 0.07 to 0.20	0.25	135
2-O-1	430	16.61	From 0.21 to 11.24	0.06	268
2-O-2	240	17.47	From 0.92 to 22.17	0.02	245
2-T	50	16.00	From 0.15 to 5.77	0.02	243
3-O	240	17.79	From 0.56 to 15.81	0.05	150
3-T	100	17.00	From 0.11 to 4.65	0.06	215
4-O	437	15.88	From 0.04 to 0.16	37.83	167
4-T	50	16.08	From 0.10 to 1.50	0.64	153
5-O	440	16.84	From 0.04 to 0.26	12.70	147
5-T-1	50	17.00	From 0.40 to 4.00	0.41	167
5-T-2	100	17.00	From 0.01 to 0.81	0.87	247
6-O-1	430	17.04	From 0.04 to 0.50	3.54	181
6-O-2	435	16.56	From 0.04 to 0.42	5.64	310
6-T-1	50	17.00	From 0.09 to 7.50	0.03	252
6-T-2	100	17.00	From 0.07 to 1.13	1.08	157

578

579 Note: First number refers to the tested gradation and the last one is the specimen

580 number; O = oedo-permeameter; T = triaxial erodimeter

581

582 **Table 3** Critical Hydraulic Gradient and Erosion Coefficient

Specimen reference in paper	Critical hydraulic gradient i_c (-)	Erosion coefficient 10^{-5} (s.m ⁻¹)
1-O	0.096	1.22
1-T	0.110	0.03
2-O-1	/	/
2-O-2	/	/
2-T	4.000	/
3-O	/	/
3-T	1.200	/
4-O	0.075	/
4-T	0.130	/
5-O	0.075	0.58
5-T-1	1.600	/
5-T-2	0.120	0.05
6-O-1	0.085	1.19
6-O-2	/	0.25
6-T-1	/	/
6-T-2	0.100	0.18

583 Notes: / = determination not possible for considered specimen

584

585

586 **Table 4** Cumulative Loss Dry Mass, Cumulative Expended Energy, Erosion
587 Resistance Index and Suffusion Susceptibility Classification

Specimen reference in paper	Cumulative Loss Dry Mass (kg)	Cumulative Expended Energy (J)	Erosion Resistance Index (-)	Suffusion susceptibility classification
1-O	1.2473	1087.90	2.94	E
1-T	0.00049	0.38	2.89	E
2-O-1	0.0231	385.20	4.22	MR
2-O-2	0.0176	298.14	4.23	MR
2-T	0.00001	0.30	4.48	MR
3-O	0.0234	1011.93	4.64	MR
3-T	0.00016	8.66	4.73	MR
4-O	0.8434	971.35	3.06	ME
4-T	0.00087	1.59	3.26	ME
5-O	0.5138	1167.67	3.36	ME
5-T-1	0.00114	9.52	3.92	ME
5-T-2	0.00034	2.55	3.88	ME
6-O-1	1.8778	1666.80	2.95	E
6-O-2	1.6787	2020.55	3.08	ME
6-T-1	0.00039	1.94	3.70	ME
6-T-2	0.00184	7.00	3.59	ME

588

589 Note: MR = Moderately Resistant; ME = Moderately Erodible; E = Erodible

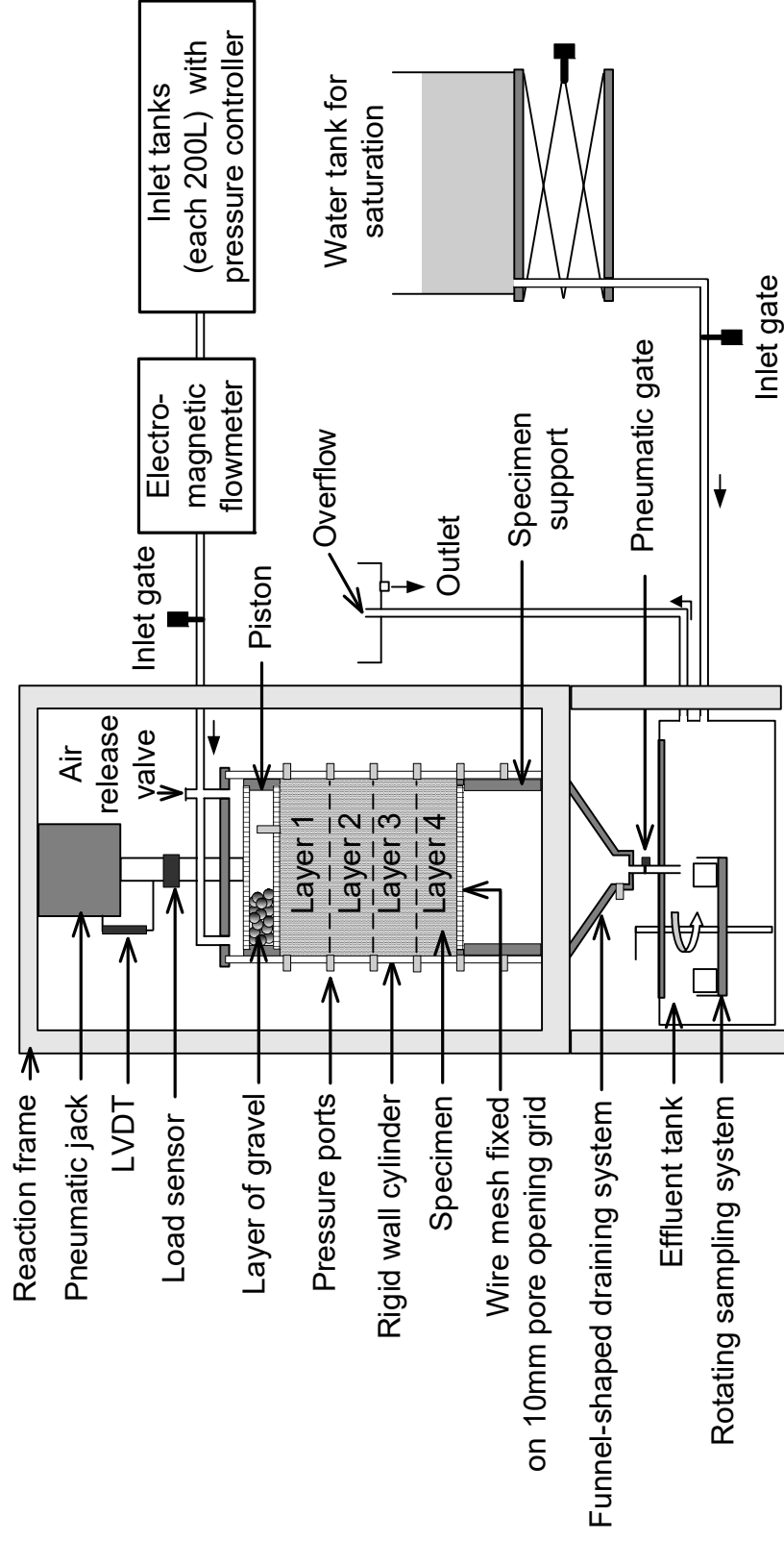


Figure 1 (a)

Figure 1 (b)

Zhong C., Le V.T., Bendahmane F., Marot D., Yin Z.Y. (2018). Investigation of spatial scale effects on suffusion susceptibility. Journal of Geotechnical and Geoenvironmental Engineering (ASCE), 144(9): 04018067. DOI: 10.1061/(ASCE)GT.1943-5606.0001935.

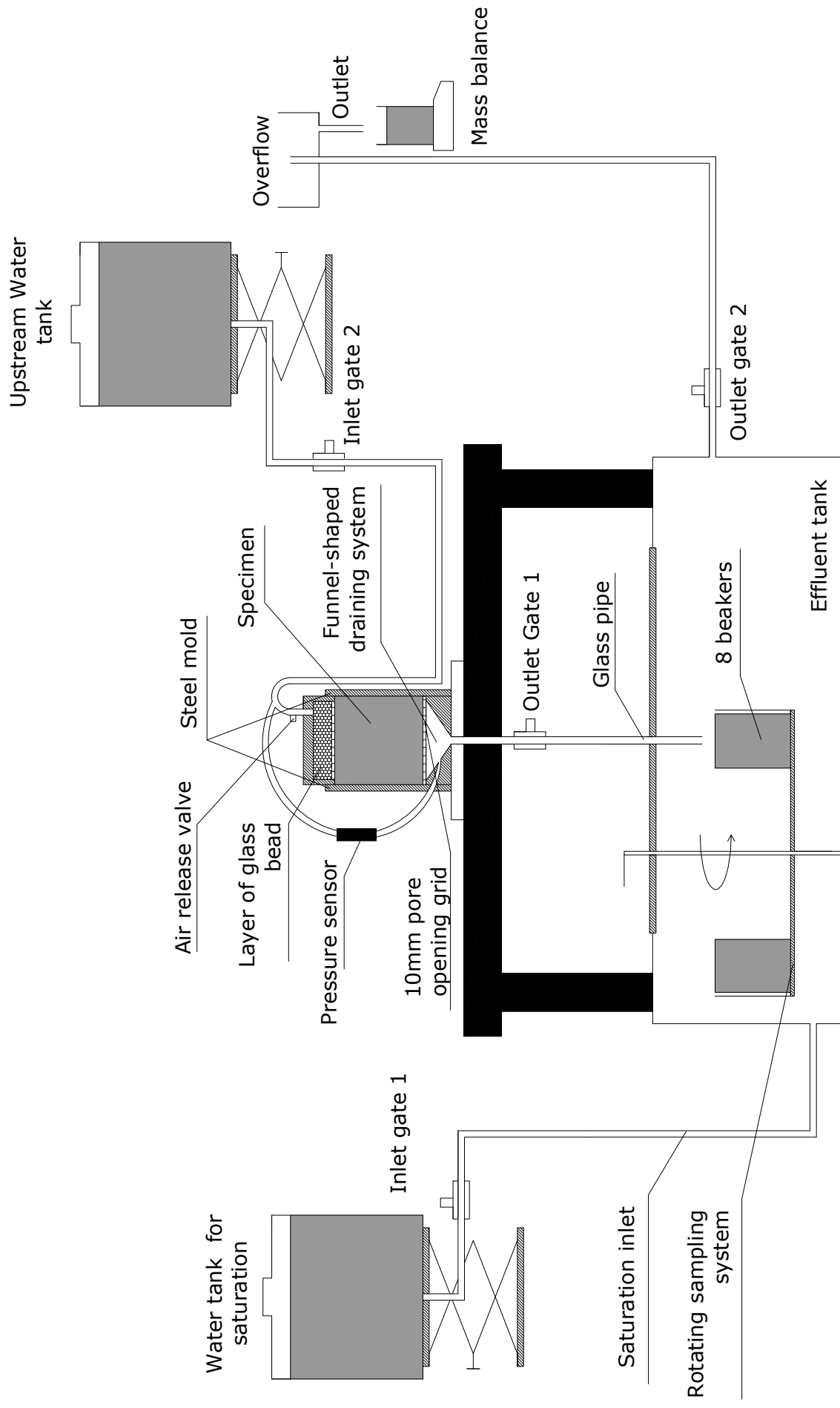
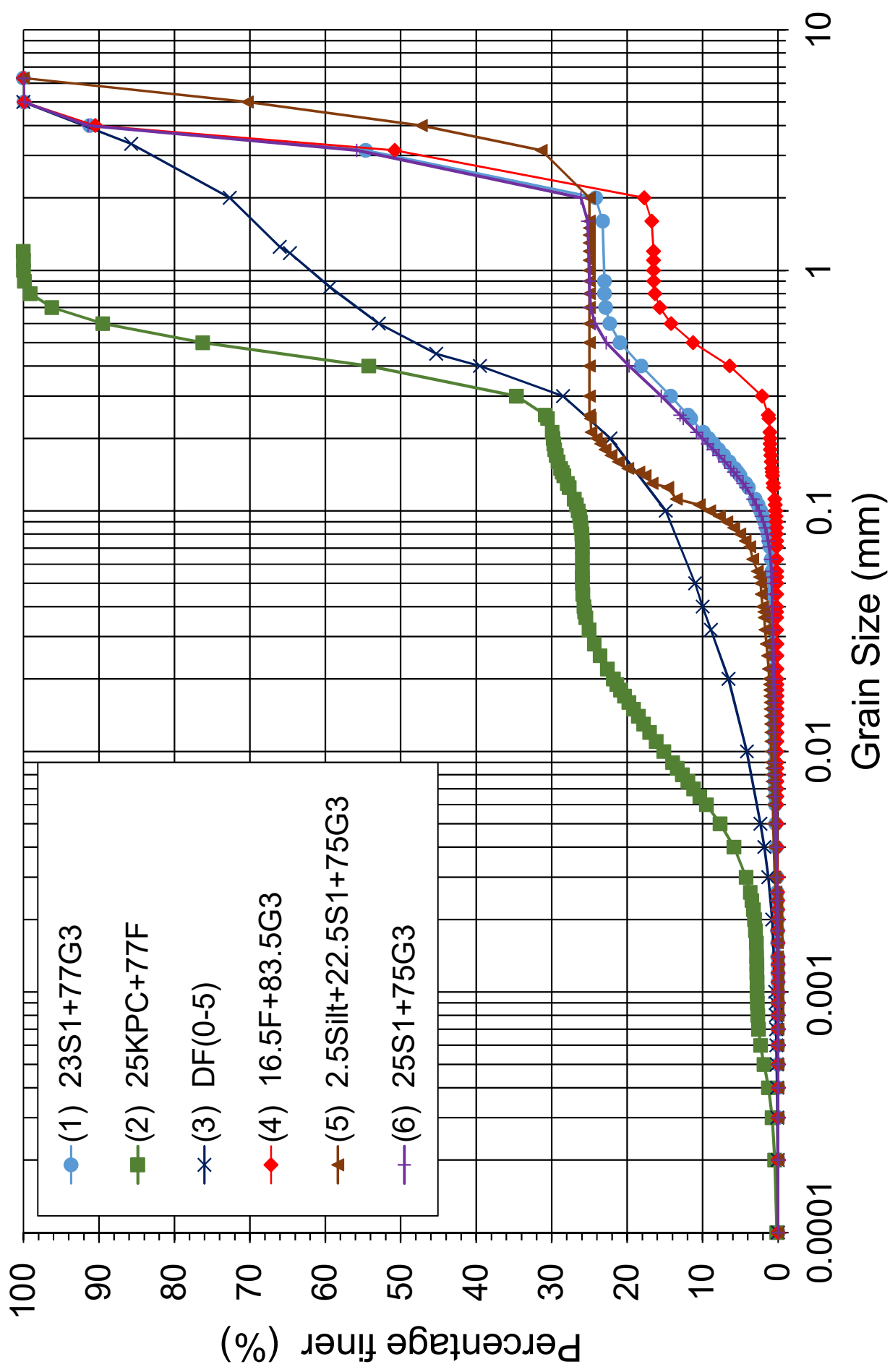


Figure 2

Zhong C., Le V.T., Bendahmane F., Marot D., Yin Z.Y. (2018). Investigation of spatial scale effects on suffusion susceptibility. Journal of Geotechnical and Geoenvironmental Engineering (ASCE), 144(9): 04018067. DOI: 10.1061/(ASCE)GT.1943-5606.0001935.



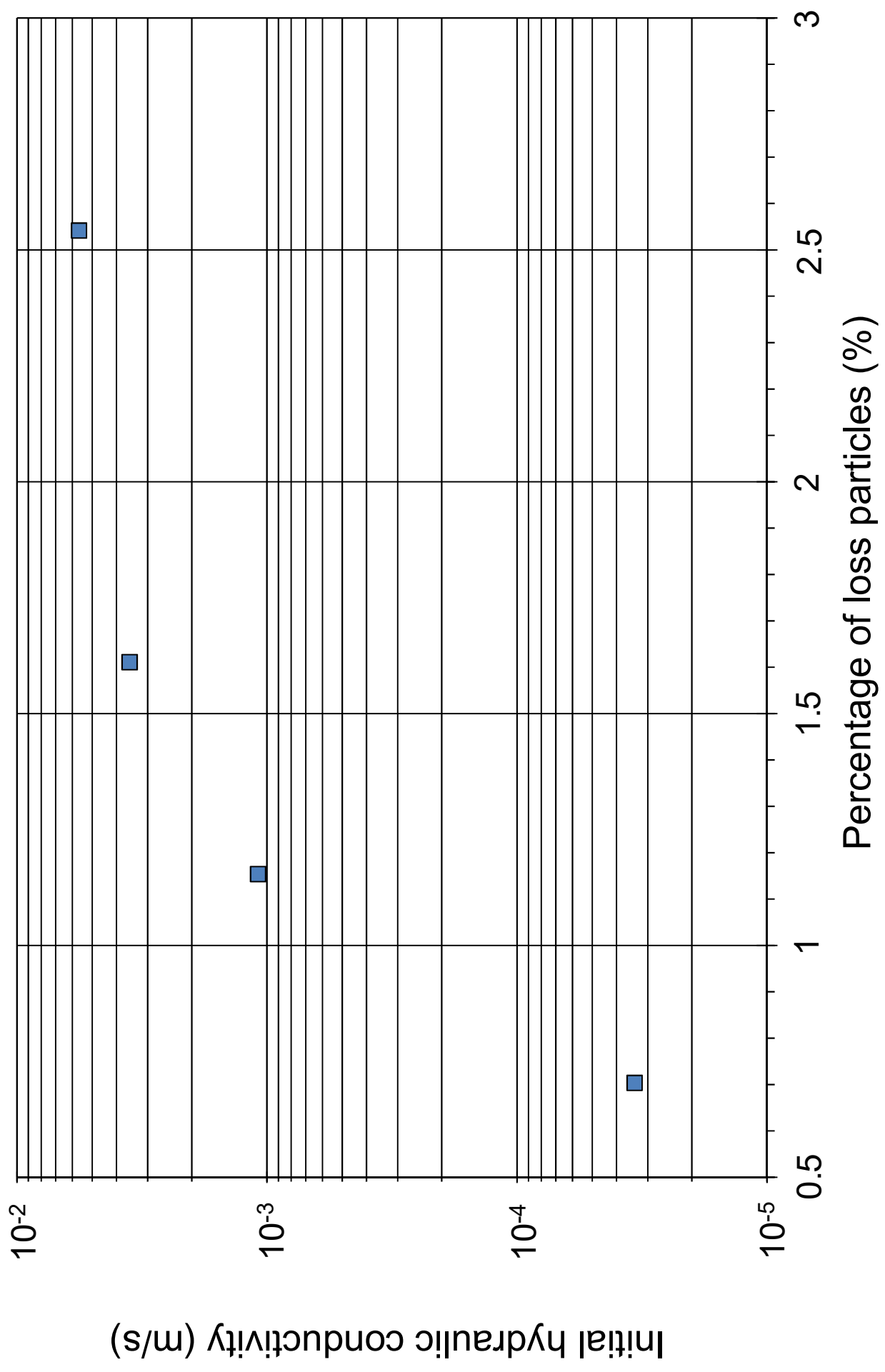
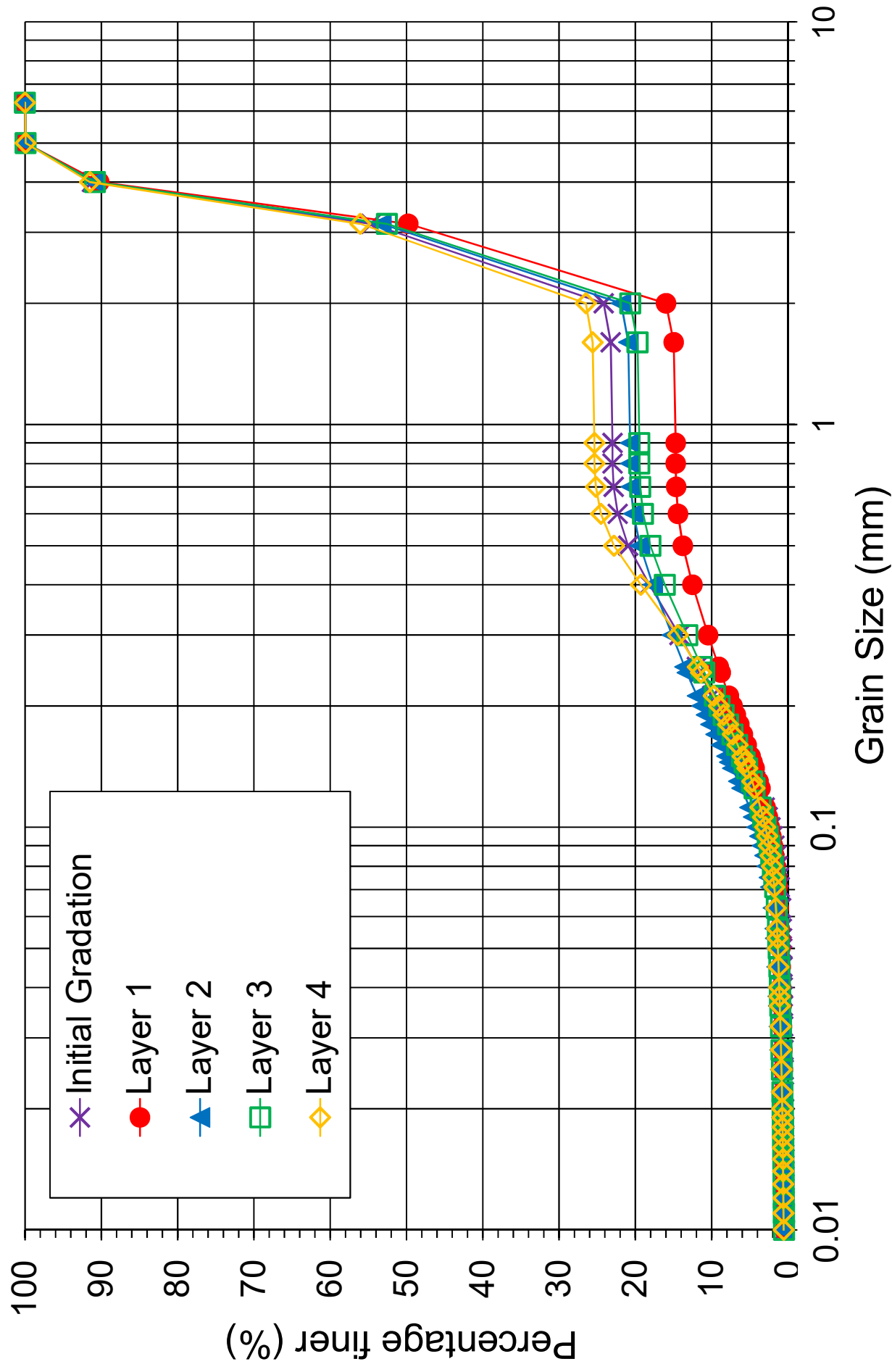


Figure 3

Figure 4 (a)

Zhong C., Le V.T., Bendahmane F., Marot D., Yin Z.Y. (2018). Investigation of spatial scale effects on suffusion susceptibility. Journal of Geotechnical and Geoenvironmental Engineering (ASCE), 144(9): 04018067. DOI: 10.1061/(ASCE)GT.1943-5606.0001935.



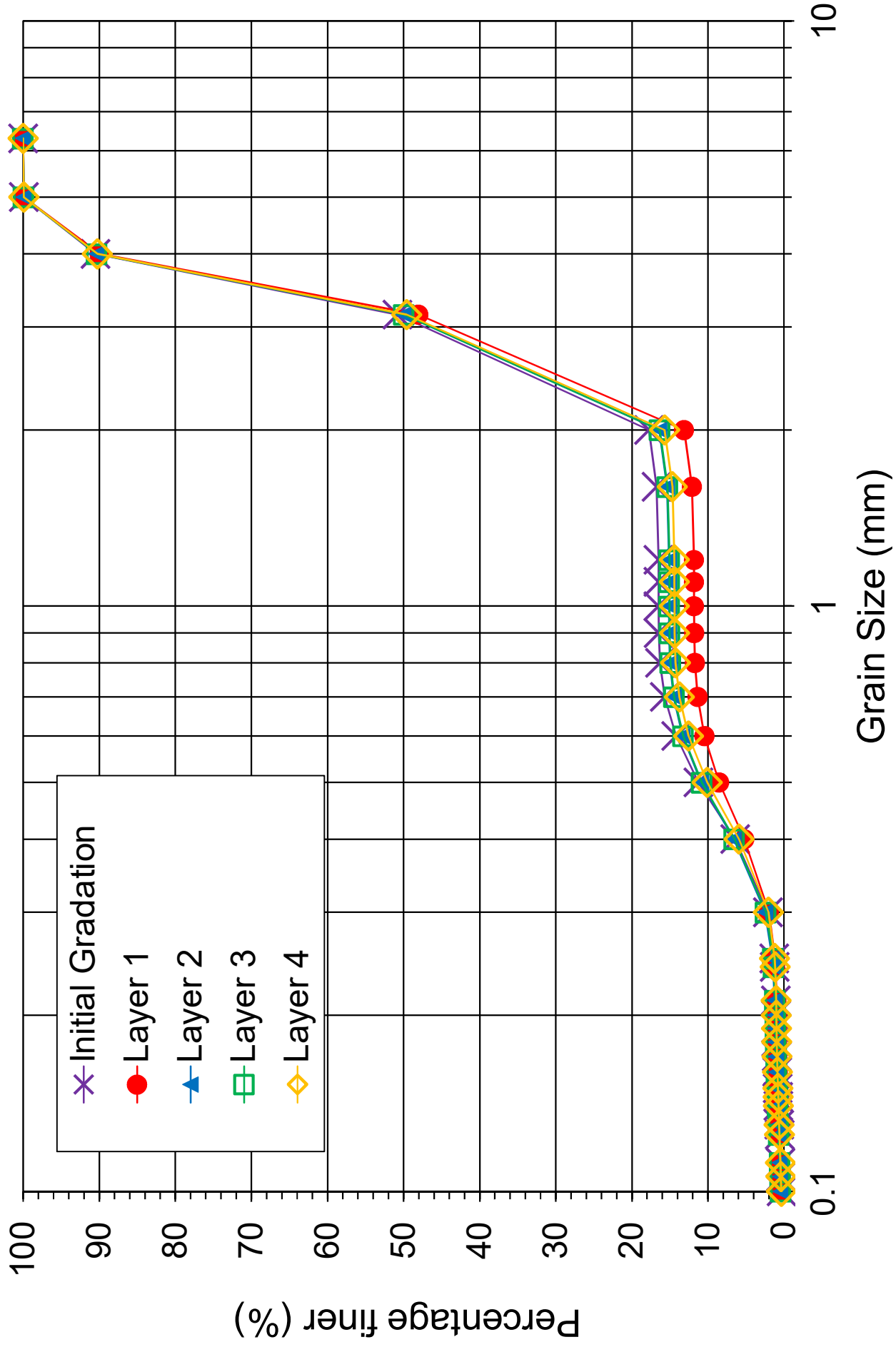


Figure 4 (b)

Figure 5

Zhong C., Le V.T., Bendahmane F., Marot D., Yin Z.Y. (2018). Investigation of spatial scale effects on suffusion susceptibility. Journal of Geotechnical and Geoenvironmental Engineering (ASCE), 144(9): 04018067. DOI: 10.1061/(ASCE)GT.1943-5606.0001935.

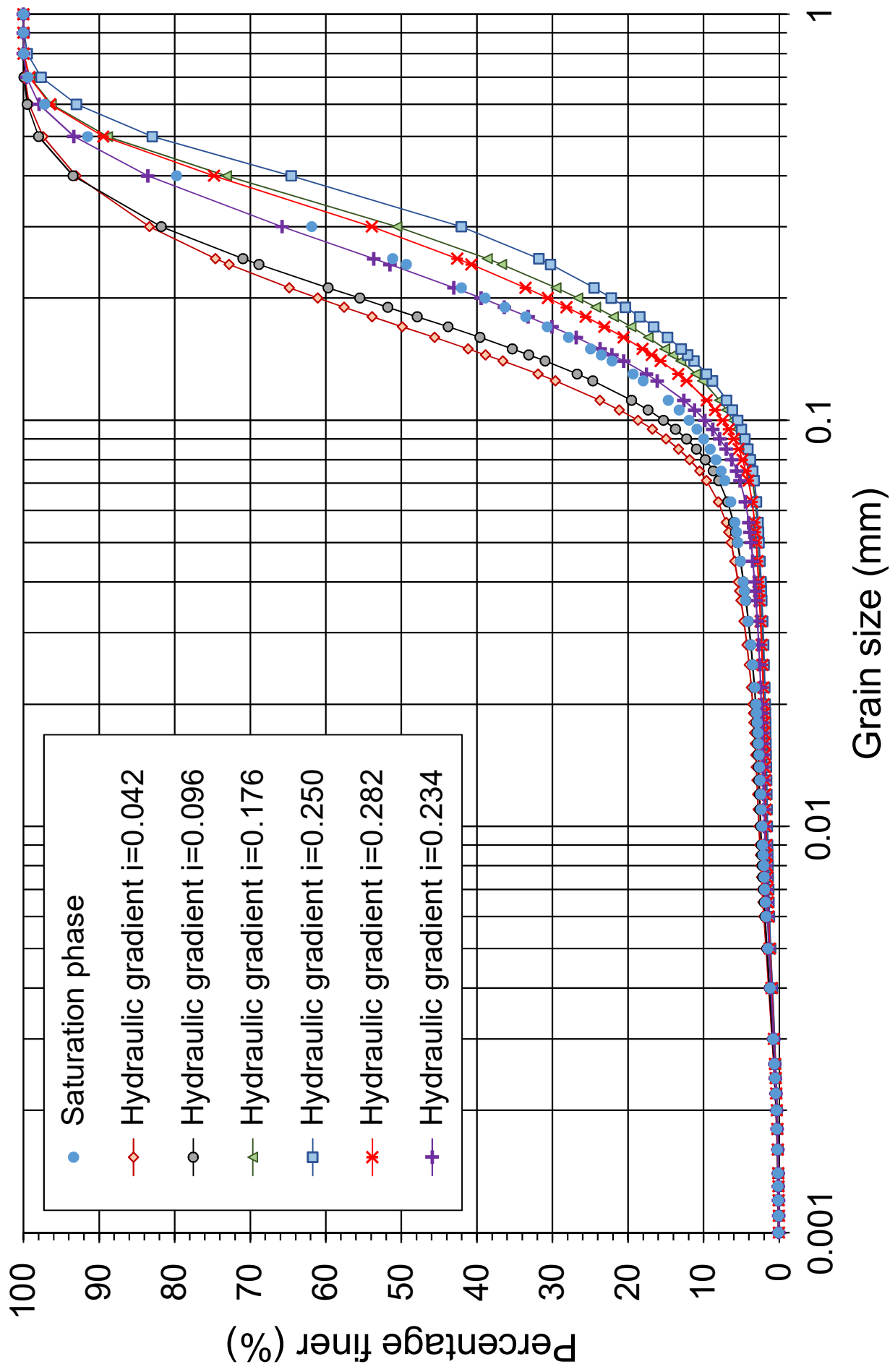


Figure 6 (a)

Zhong C., Le V.T., Bendahmane F., Marot D., Yin Z.Y. (2018). Investigation of spatial scale effects on suffusion susceptibility. Journal of Geotechnical and Geoenvironmental Engineering (ASCE), 144(9): 04018067. DOI: 10.1061/(ASCE)GT.1943-5606.0001935.

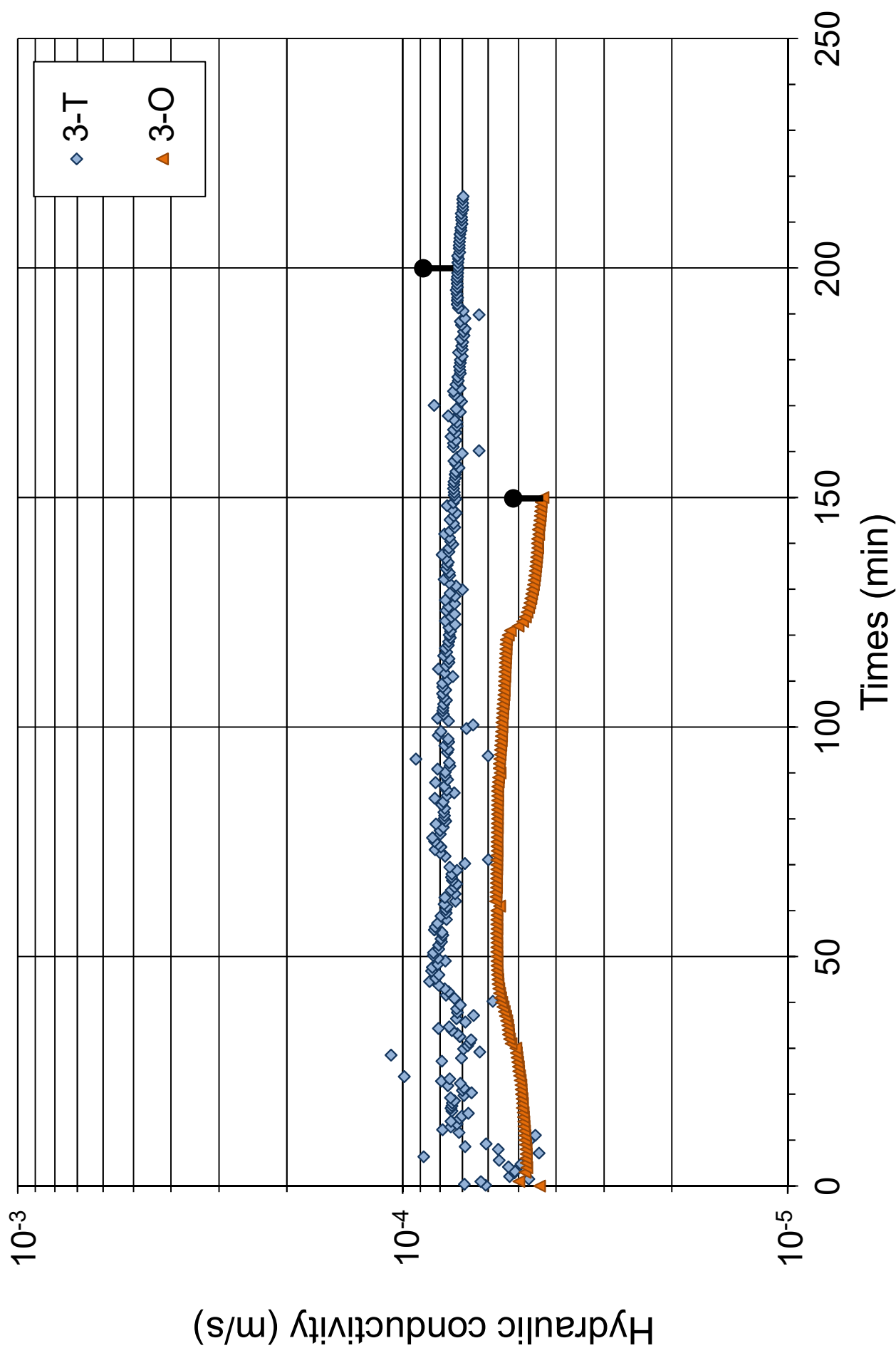


Figure 6 (b)

Zhong C., Le V.T., Bendahmane F., Marot D., Yin Z.Y. (2018). Investigation of spatial scale effects on suffusion susceptibility. Journal of Geotechnical and Geoenvironmental Engineering (ASCE), 144(9): 04018067. DOI: 10.1061/(ASCE)GT.1943-5606.0001935.

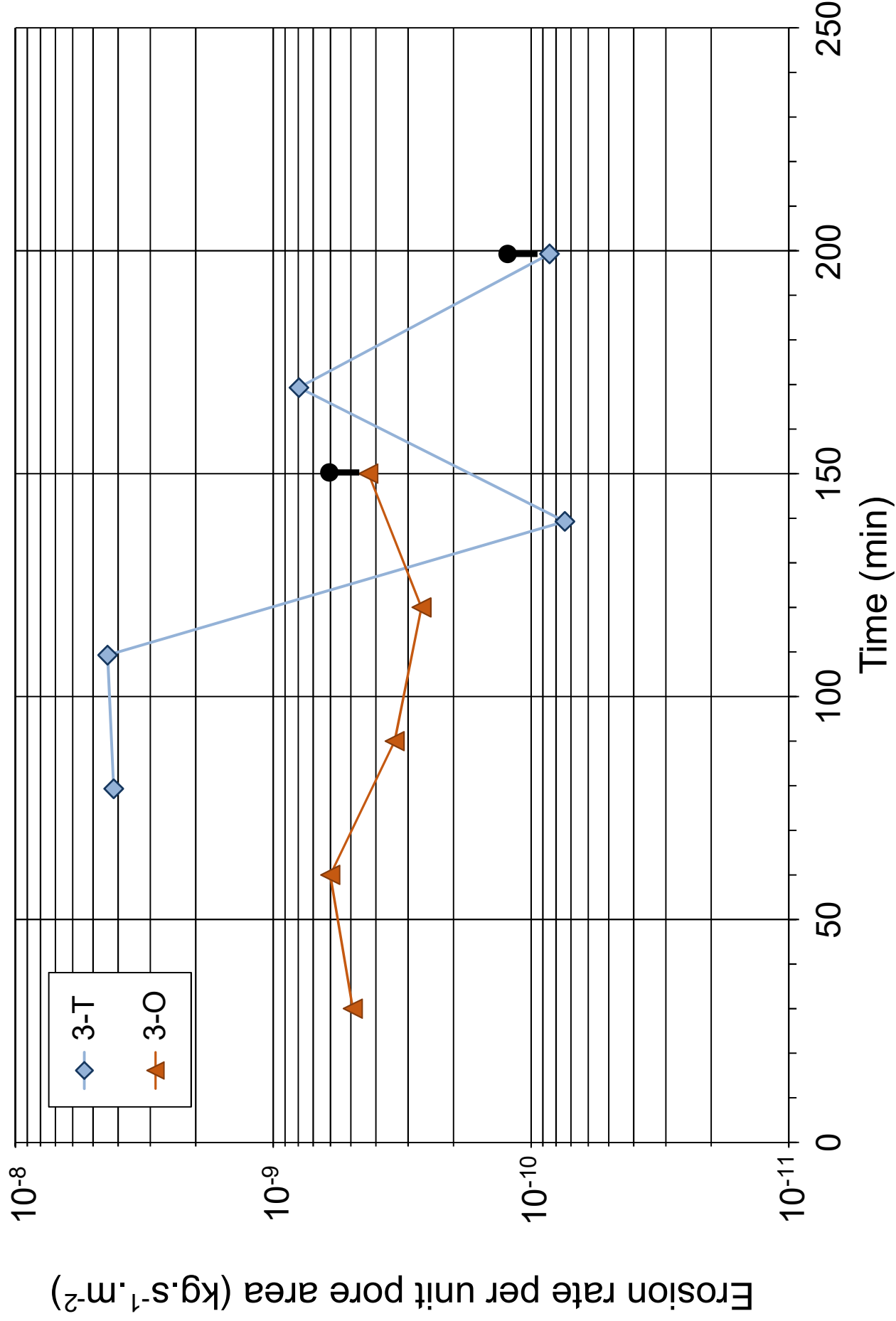
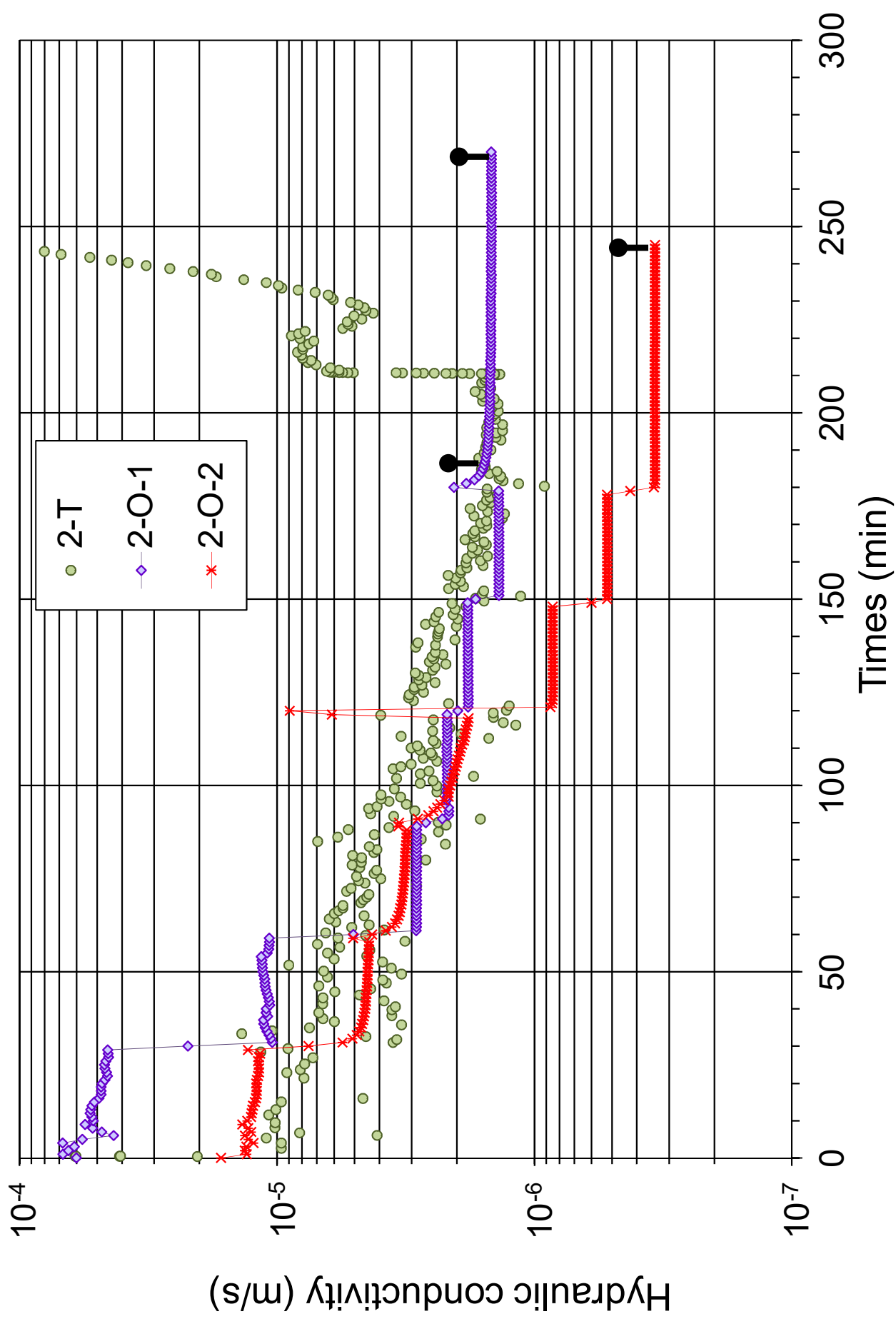


Figure 7 (a)

Zhong C., Le V.T., Bendahmane F., Marot D., Yin Z.Y. (2018). Investigation of spatial scale effects on suffusion susceptibility. Journal of Geotechnical and Geoenvironmental Engineering (ASCE), 144(9): 04018067. DOI: 10.1061/(ASCE)GT.1943-5606.0001935.



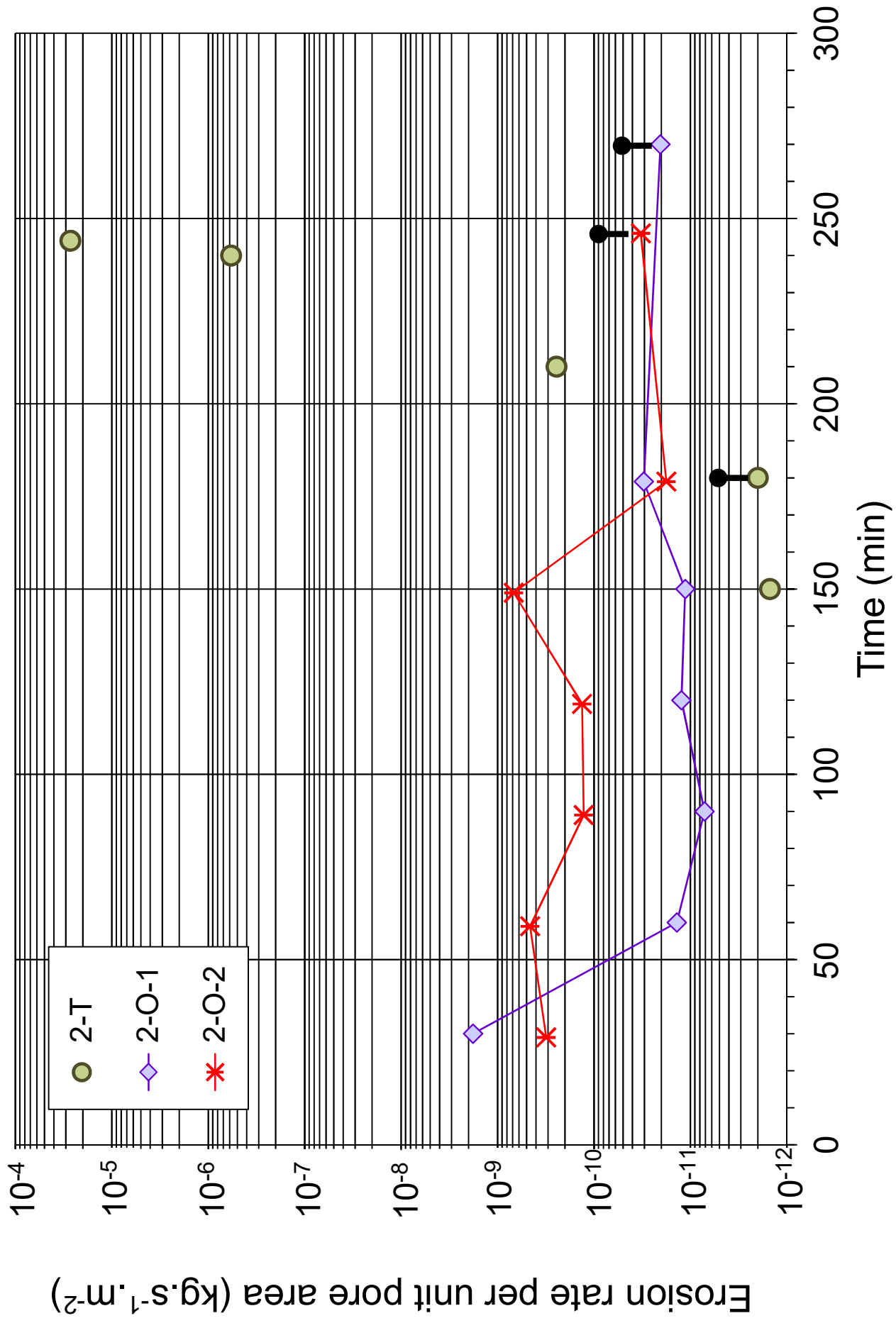


Figure 7 (b)

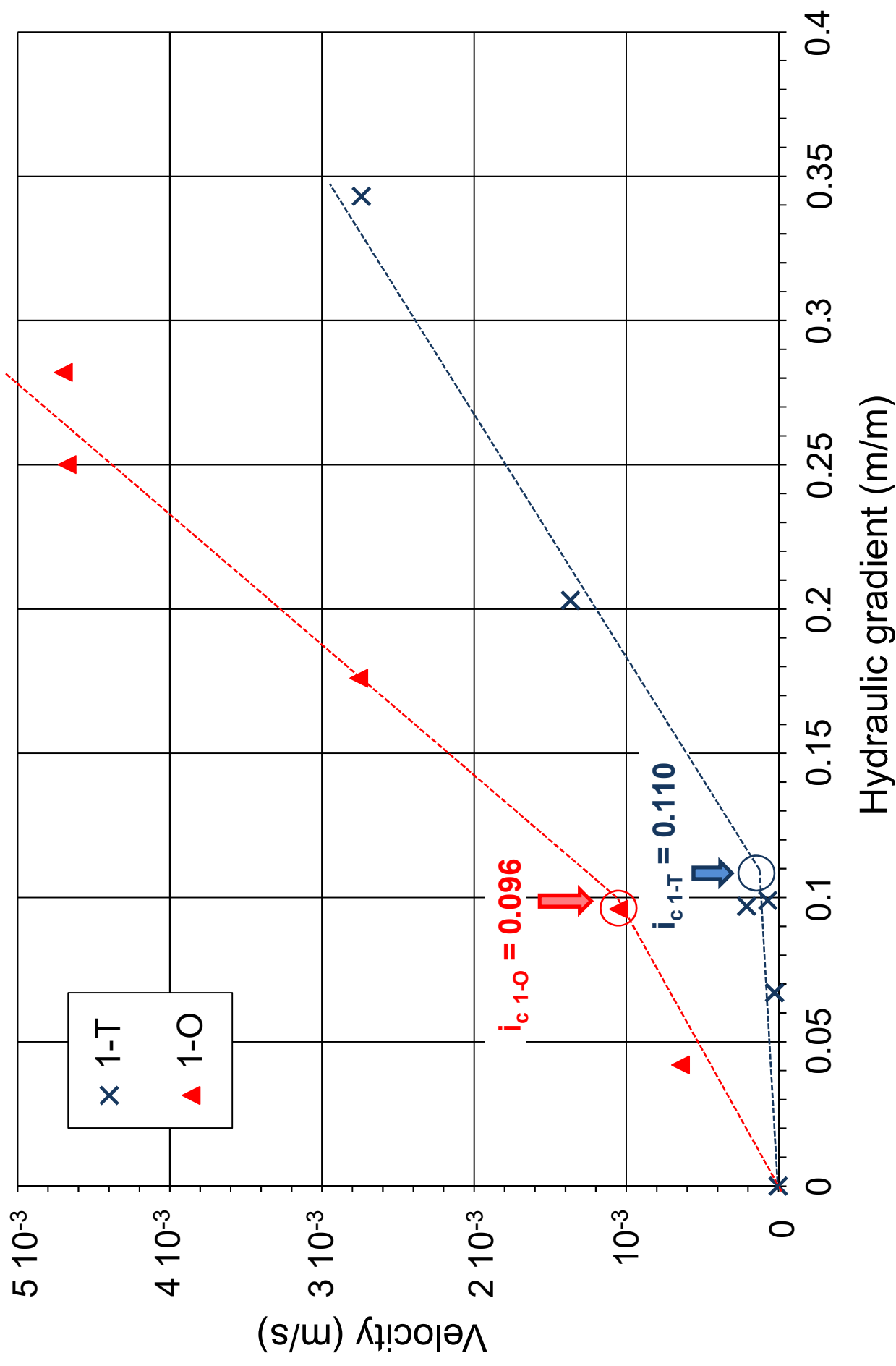


Figure 8 (a)

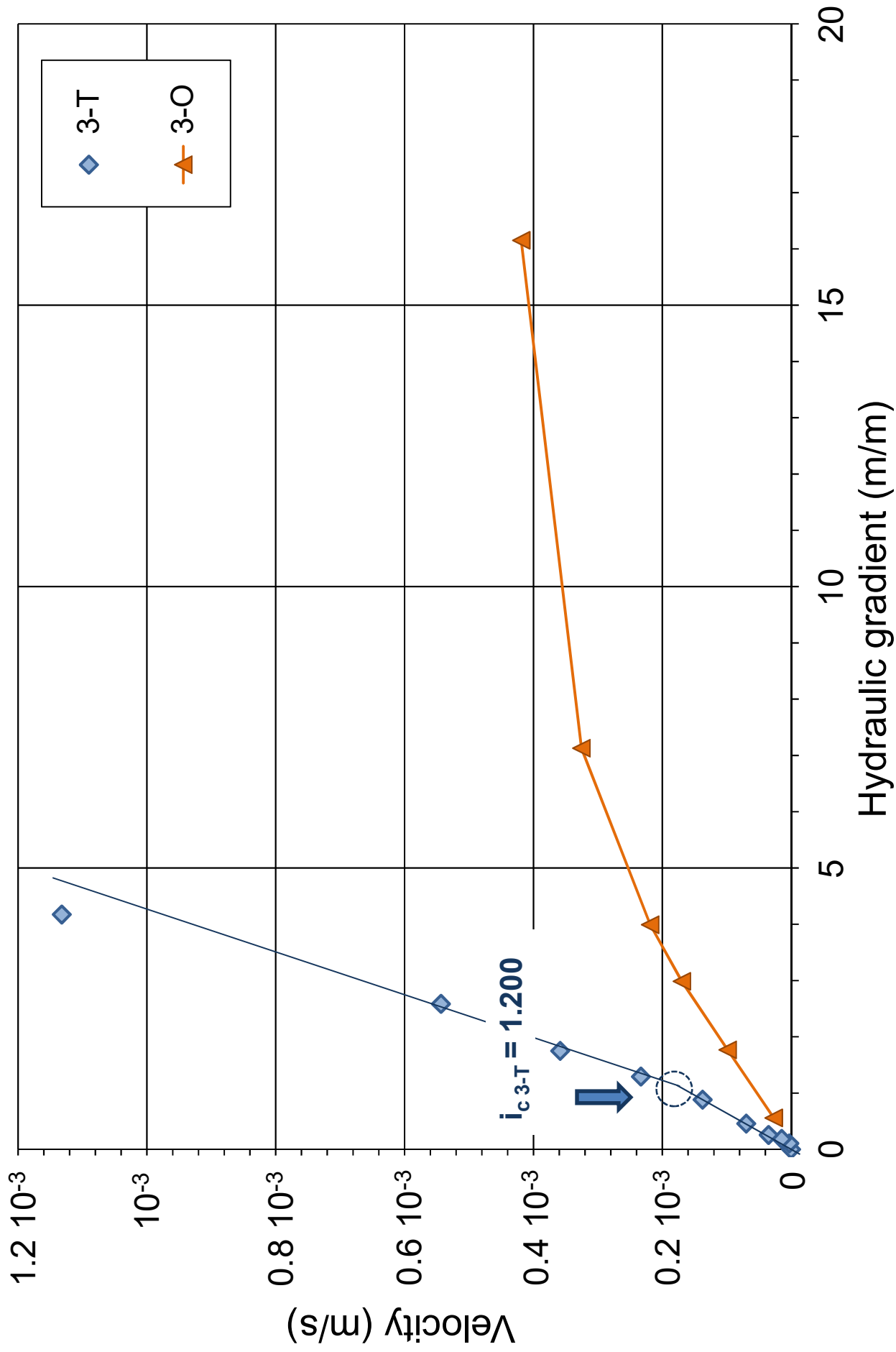


Figure 8 (b)

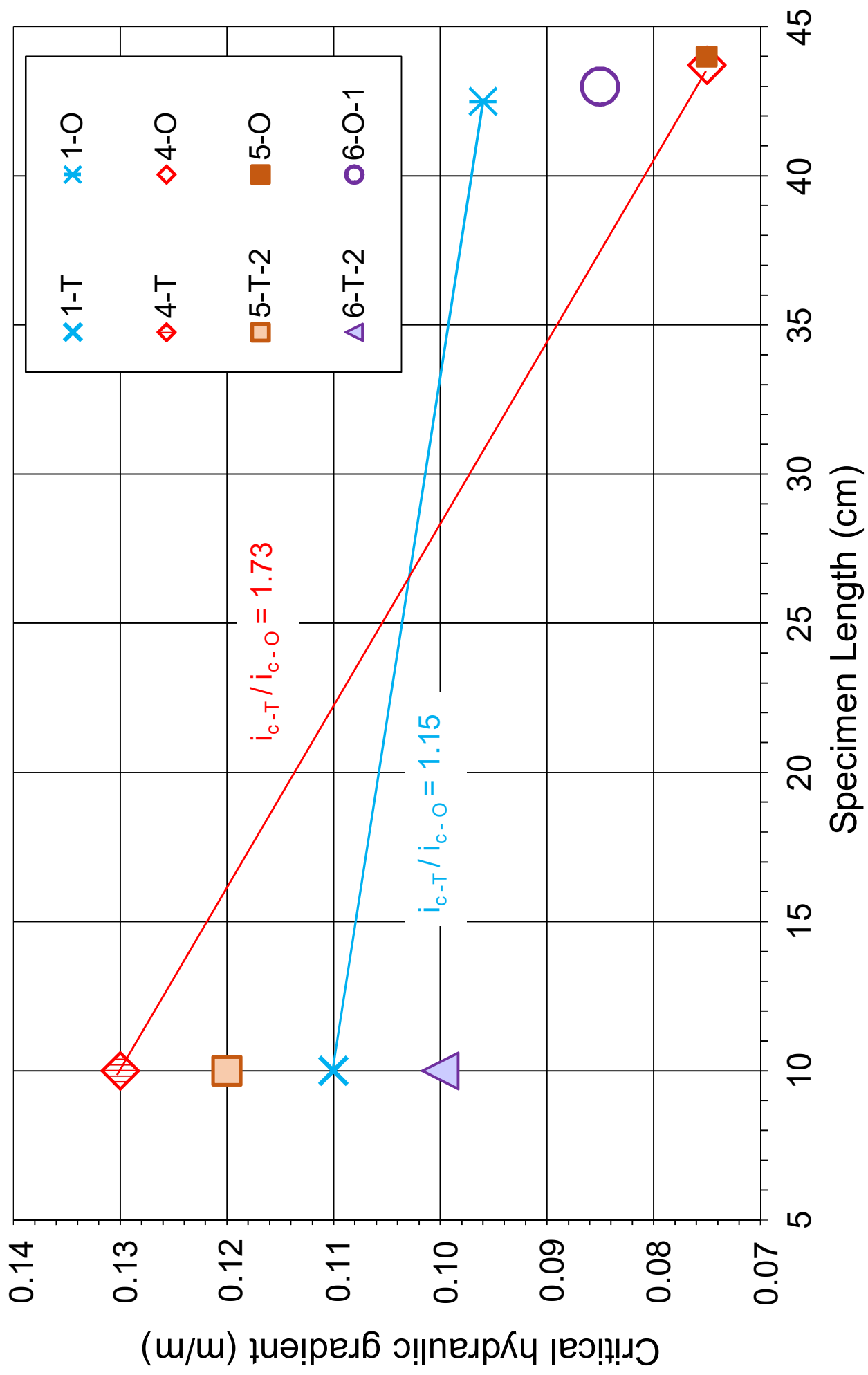


Figure 9

Figure 10 (a)

Zhong C., Le V.T., Bendahmane F., Marot D., Yin Z.Y. (2018). Investigation of spatial scale effects on suffusion susceptibility. Journal of Geotechnical and Geoenvironmental Engineering (ASCE), 144(9): 04018067. DOI: 10.1061/(ASCE)GT.1943-5606.0001935.

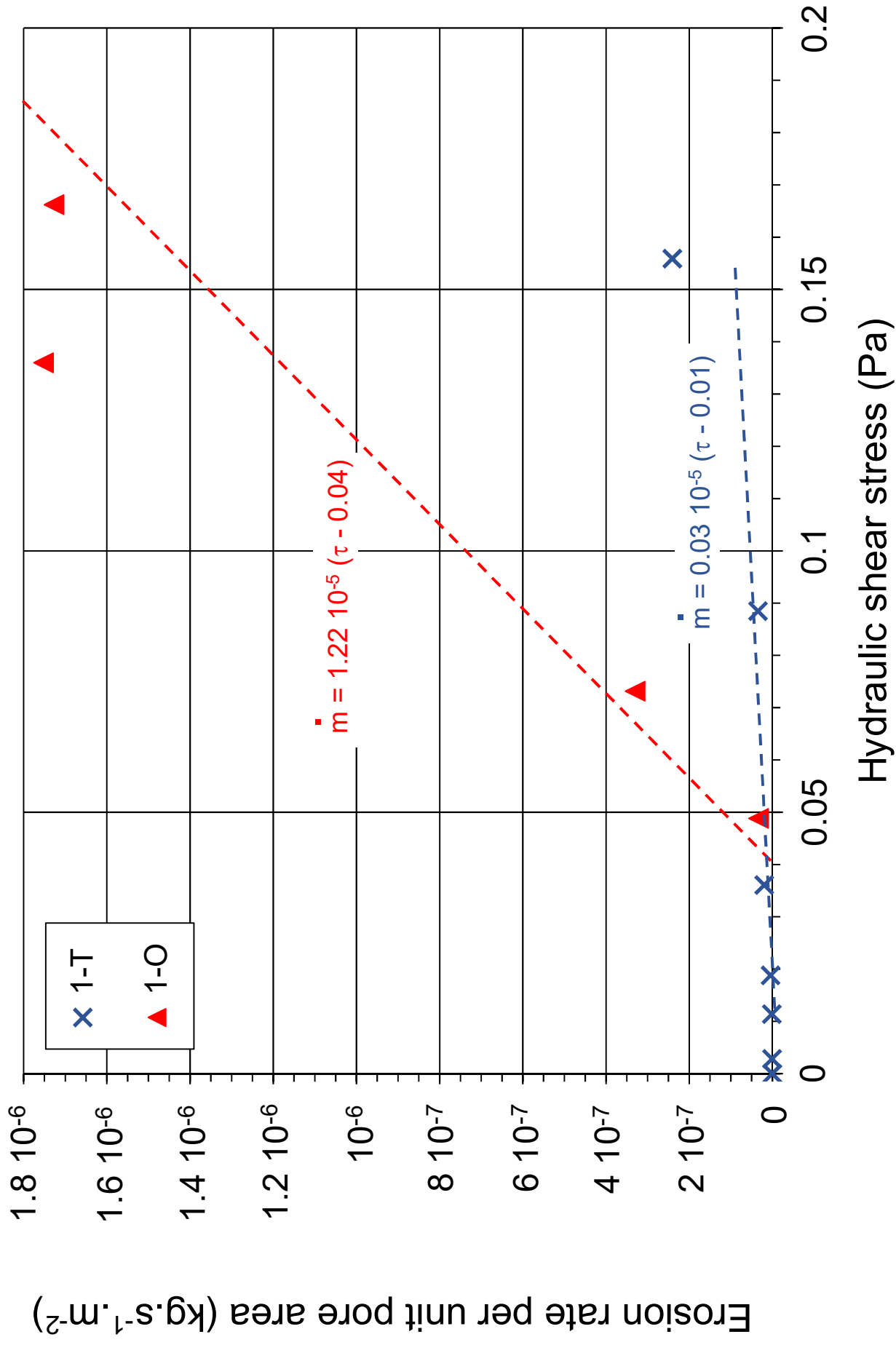
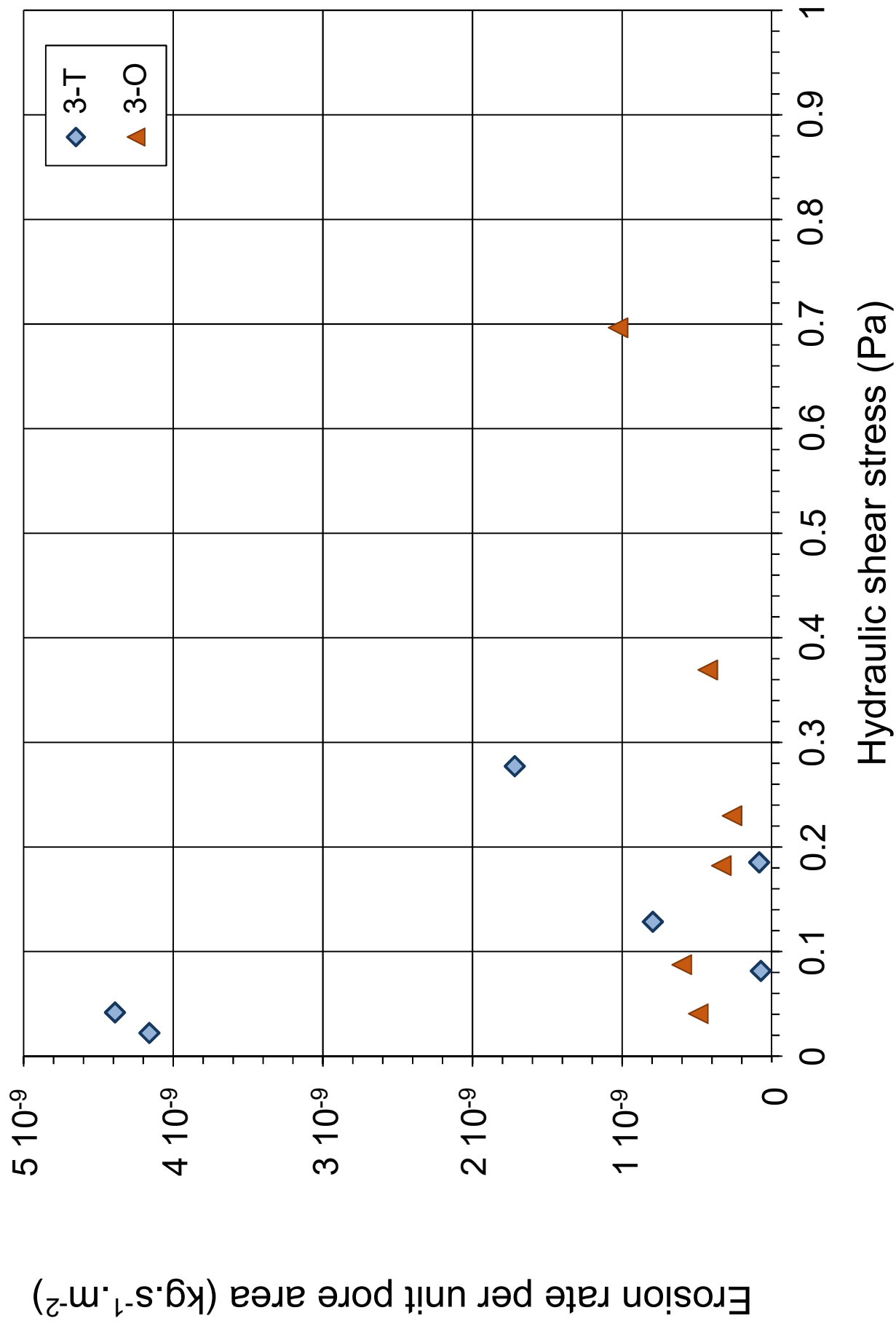


Figure 10 (b)

Zhong C., Le V.T., Bendahmane F., Marot D., Yin Z.Y. (2018). Investigation of spatial scale effects on suffusion susceptibility. Journal of Geotechnical and Geoenvironmental Engineering (ASCE), 144(9): 04018067. DOI: 10.1061/(ASCE)GT.1943-5606.0001935.



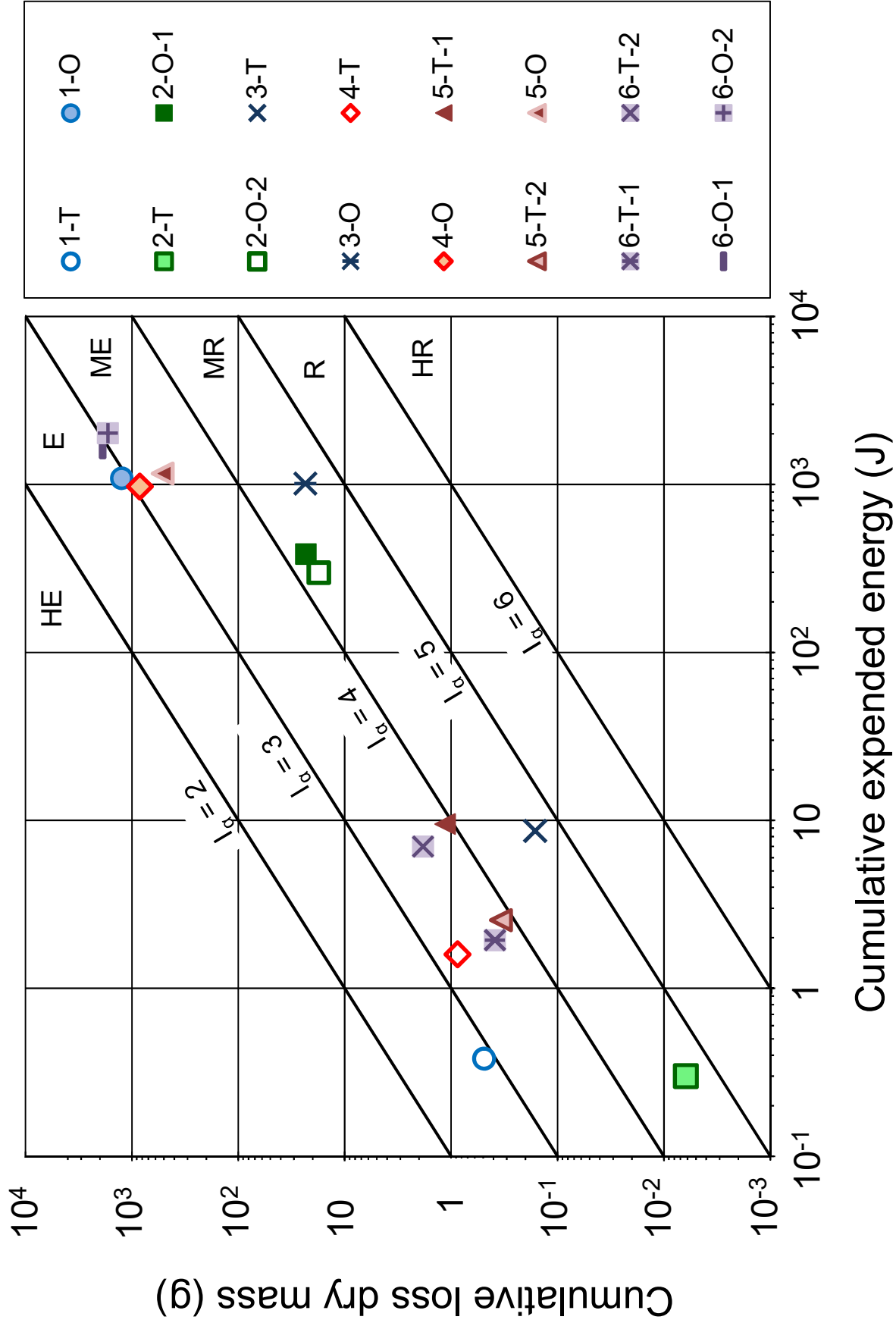


Figure 11